ANL-GenIV-076

Enhancement of REBUS-3/DIF3D for Whole-Core Neutronic Analysis of Prismatic Very High Temperature Reactor (VHTR)

C. H. Lee, Z. Zhong, T. A. Taiwo, W. S. Yang, H. S. Khalil, M. A. Smith

Nuclear Engineering Division
Argonne National Laboratory
9700 South Cass Avenue
Argonne, IL 60439

September 30, 2006

TABLE OF CONTENTS

LIST OF TABLES

LIST OF FIGURES

ABSTRACT

Enhancements have been made to the REBUS-3/DIF3D code suite to facilitate its use for the design and analysis of prismatic Very High Temperature Reactors (VHTRs). A new cross section structure, using table-lookup, has been incorporated to account for cross section changes with burnup and fuel and moderator temperatures. For handling the new cross section format, the NEUTRONXS, COMPACTSCAT, and GENERALISOTOPE modules have been developed in REBUS-3 using FORTRAN 90/95 object-oriented data structures. These modules provide a cross section storage procedure, construct microscopic cross section data for all isotopes, and contain a single block of banded scattering data for efficient data management. In addition, fission products except I, Xe, Pm, and Sm, can be merged into a single lumped fission product to save storage space, memory, and computing time during REBUS-3 fuel cycle analysis without sacrificing depletion solution accuracy.

A simple thermal-hydraulic (thermal-fluid) feedback model has been developed for prismatic VHTR cores and implemented in REBUS-3 for temperature feedback calculations. The axial conduction term was neglected in the formulation because of its small gradient, compared to the corresponding radial temperature gradient. With the simple model, the average fuel and graphite temperatures are accurately estimated compared to reference STAR-CD results. The feedback module is currently working for the non-equilibrium fuel cycle analysis option of REBUS-3. Future work should include the extension of this capability to the equilibrium cycle option of the code and additional verification of the feedback module.

For the simulation of control rods in VHTR cores, delta-macroscopic cross sections have been defined to account for the effect of control rod insertion. The REBUS-3 code has been modified to use the cross sections when control rods are inserted in a calculation node.

In order to represent asymmetric core blocks (e.g., fuel blocks or reflector blocks containing asymmetric absorber rods), surface-dependent discontinuity factors based on nodal equivalence theory have been introduced into the nodal diffusion theory option of the DIF3D code (DIF3D-nodal) to systematically correct the nodal cross sections. In parallel, the

discontinuity factors based on the Simplified Equivalence Theory (SET) have been incorporated for all nodal options: DIF3D-nodal and DIF3D-VARIANT (nodal transport capability).

Two- and three-dimensional core calculations have been performed using the routines developed and modified in this work and the cross sections generated from single fuel block and one-dimensional or two-dimensional fuel-reflector model. Generally, REBUS-3/DIF3D results for the core multiplication factor and power distribution are found to be in good agreement with MCNP results particularly when discontinuity factors are applied. It is also shown that the DIF3D-VARIANT option provides a better spatial solution in its diffusion approximation than the DIF3D-nodal option. In addition, it is observed that control rod worths can be estimated within an acceptable range compared to MCNP results. However, the core power tilt needs to be improved by introducing surface-dependent discontinuity factors. It is thus concluded that future work should include the incorporation of nodal equivalence parameters for the DIF3D-VARIANT option or the improvement of the spatial approximation of the DIF3D-nodal option.

1.0 INTRODUCTION

Both prismatic block and pebble-bed designs are being considered in the U.S. and internationally for the cores of Very High Temperature Reactors (VHTRs). In the USDOE VHTR/NGNP Program, Argonne has been assigned the task of developing a deterministic neutronic code suite for routine analysis and design of prismatic VHTRs. This work is being done with a collection of existing capabilities (relying on their validation bases where pertinent), with the goal of providing the required capabilities at modest cost.

In the prismatic VHTR design, the core is composed radially of rings of hexagonal graphite fuel and reflector elements, and reactivity control materials. The fuel elements have channels for fuel and burnable poison compacts, helium coolant flow, control rod passages, and fuel element handling. [1, 2] The cylindrical fuel compacts contain coated fuel particles (CFPs) dispersed in the graphite matrix of the compact. Several graphite fuel elements (typically 10) are stacked vertically to make a fuel column. Inner and outer core rings contain permanent/removable graphite reflector columns. These reflector columns surround a few rings of fuel columns (typically 3) in the core inner annulus. The annular core design was found necessary to support the passive safety requirement for the VHTR.

The heterogeneity effect (termed double heterogeneity effect) arising from the use of the CFPs should be adequately represented in the lattice physics code utilized for the analysis of the prismatic VHTR cores in order to obtain accurate results for the core criticality state. This effect has been found to be about 2-4% $\Delta k/k$ (reactivity) in VHTR assemblies/cores using enriched uranium fuels, and about 10-15% $\Delta k/k$ for those using transuranics fuels as in the deep-burn concepts. The lattice physics code should also be able to provide accurate values for the single-assembly power distribution and multiplication factor, in addition to the assembly/zone average cross section data it produces. The whole-core analysis tool should be able to model very accurately the core reactivity, flux and power distributions, accounting for the severe flux gradients and power peaking at the core and reflector interfaces. Local neutron streaming effects arising from the large control rod holes should be accurately represented. The core depletion state (including the nuclide number densities and core burnup distribution) should also be accurately predicted. These core physics parameters have direct impact on thermal-fluids/safety analysis,

fuels and materials designs, and plant economics. Additionally, the code suite should be computationally efficient in order to perform the large number of calculations required to support core scoping analysis and detailed designs in reasonable time.

A whole-core transport capability using stochastic or deterministic transport theory solution method would be desirable for modeling VHTR cores accurately, eliminating the cumbersome and complex tasks of lattice cross section generation, condensation, functionalization, local information recovery, etc. Currently, however, no such capability exists that has detailed thermal feedback model, depletion option, and can give whole-core solutions in reasonable time. Therefore, practical computational tools for VHTR design and analysis are based on the conventional two-step deterministic lattice and whole-core calculation approaches, which have been used successfully in the light water reactor (LWR) industry, with recognition that there are significant differences between the LWRs and graphite moderated systems. Some of the differences include the core and assembly geometries, fuel type, fuel average burnups, thermal feedback mechanism, difference between core outlet and inlet temperatures, core average temperatures, neutron mean free paths, neutron streaming, etc.

Based on previous studies [3, 4], Argonne has selected the DRAGON code for lattice physics calculations, and the REBUS-3 and DIF3D codes for whole-core calculations. In addition to its lattice capabilities, the DRAGON code has a capability for representing explicitly the coated fuel particles at the assembly level, and additionally it is free software. [5] In the event that future evaluations show the code to be costly to upgrade to the necessary quality assurance (QA) level, the WIMS9 code could be used as backup; this latter code also represents coated fuel particles, but however it is a vendor code and comes with cost, particularly to obtain the source code.

Separately, because the REBUS-3 and DIF3D codes together provide an accurate and efficient multigroup and multidimensional (including hexagonal-Z) capability for fuel cycle analysis, they were selected for the code suite; note that DIF3D serves as the module for multiplication factor, and flux and power distribution calculations, and REBUS-3 the module for depletion and fuel cycle calculations. [6, 7] Thus, the code suite based on DRAGON and REBUS-3/DIF3D has been adapted for the analysis of prismatic VHTRs, with the expectation

that the integration of the codes could be done with a smaller amount of effort compared to other codes. The recent improvements to the code suite that pertain to the DRAGON code have been presented in a companion report (Reference 8), and will not be revisited in this report. An overview of the VHTR code suite is presented in Section 2.0.

Required modifications to REBUS-3/DIF3D have been identified for VHTR core simulation. Cross section manipulation modules need to be updated to accommodate a new cross section tabulation/functionalization scheme that uses burnup and temperatures as the independent variables. A thermal-hydraulics (thermal-fluid) module should be incorporated to calculate accurately the fuel and graphite temperatures used for thermal feedback calculations. A control rod simulation module representative of the VHTR design needs to be incorporated to augment the feature that exists in the code for fast reactor analysis. In addition, the routines associated with surface-dependent discontinuity factors have to be revised to use conventional nodal equivalence parameters (currently employed for LWRs). The details of those modifications are discussed in Section 3.0.

The current capabilities of the code have been demonstrated using two- and three-dimensional benchmark calculations. The results of these studies are presented in Section 4.0, where the code suite results are compared with corresponding MCNP [9] results for the multiplication factor and power distribution. The conclusions from this work and discussions on future work are provided in Section 5.0.

2.0 A CODE SUITE FOR PRISMATIC VHTR CORES

2.1 Lattice Physics Capability

The DRAGON code has been selected as the lattice physics calculation tool for the prismatic VHTR. [3] The DRAGON code has a collection of models for simulating the neutronic behavior of a unit cell or a fuel lattice in a nuclear reactor. The typical functionalities found in most modern lattice codes are contained in DRAGON. These include interpolation of microscopic cross sections supplied by means of standard libraries; resonance self-shielding calculations in multidimensional geometries; multigroup and multidimensional neutron flux calculations which can take into account neutron leakage; transport-transport or transport-diffusion equivalence calculations; and modules for editing condensed and homogenized nuclear properties for reactor calculations.

The current version of the code contains three main algorithms for the solution of the integral transport equation, ranging from a simple collision probability method coupled with the interface current method (SYBILT) to the full collision probability method (EXCELT). The code also performs isotopic depletion calculations. The code user must however supply cross sections in one of the following standard formats: DRAGON, MATXS (TRANSX-CTR), WIMSD4, WIMS-AECL, and APOLLO. Macroscopic cross sections can also be read by DRAGON via the input data stream. At ANL, the 69- and 172-group cross section libraries created in WIMSD4-format by the Reduced Enrichment for Research and Test Reactors (RERTR) project are used with the DRAGON code. The depletion chains and types of fission products to be tracked by the code are obtained from the cross section library used. For the DRAGON calculations, cross section data for the heavy nuclides are tabulated at different temperatures (2-4 points) and all the heavy nuclides contained in the library are treated as resonance materials.

An attractive feature of the DRAGON code is its ability to treat CFPs in a fuel compact during a full-assembly calculation. This capability has been used for modeling the fuel block of prismatic high-temperature gas-cooled thermal reactors and the pebble elements in alternative pebble-bed concepts.

It is noted that in the DRAGON full-assembly model for the VHTR/NGNP hexagonal block, the block is formed by a collection of pin-cell sized hexagons. Each pin-cell contains the fuel compact and its surrounding block graphite. When all the fuel and coolant-hole pin-cells are represented, the block graphite content is not totally accounted for and therefore an extra ring of pin-cell sized hexagons is used to represent the remaining graphite. The number density of the graphite in these peripheral cells is modified to preserve the graphite content of the assembly block. Due to the use of the pin-cell sized hexagons, the DRAGON assembly model has jagged boundaries, not the flat boundaries of the actual hexagonal block.

Limitations of the current version of DRAGON for VHTR core analysis have been identified. These limitations are:

1. Lack of edits for pin power and surface fluxes and currents.
2. Use of jagged block boundary; flat hexagonal boundary is required.
3. No explicit geometry representation for large control rod channels.
4. Limited restart capability making branch-case calculations tedious.
5. No explicit treatment of CFP double heterogeneity effect with the EXCELT option.
6. No flexibility for ISOTXS filenames.

Modifications have been made to the code to provide the necessary edits for the assembly pin power distribution and the surface fluxes and currents. For item 1, the pin powers are generated consistently with the pin map in the “CELL” input of the code. Surface fluxes and currents are edited for the pertinent surface of a one-dimensional model used for generating reflector cross sections. In addition, a temporary fix has been provided for item 2; small circular regions are added to all peripheral hexagonal cells in order to approximate the surface-average fluxes of a fuel block. For item 3, the large control rod hole in the fuel element is represented by a collection of pin-cell sized hexagons, preserving the control rod content. The details of the modifications and temporary fixes are presented in Reference 8. In addition, results for the fuel block suggest that additional work is required to improve the DRAGON code accuracy for certain fuel double heterogeneity problems (cases containing enriched uranium fuel kernels with large diameter). This latter issue and items 4 to 6 have not been resolved, and should be addressed in the future for solution accuracy and flexibility.

2.2 Whole-Core Capability

A burnup module is required for depletion calculations that track the time evolution of the fuel nuclides. The transmutation equations for the heavy metals and the pertinent fission products are usually solved by the depletion module for discrete spatial zones (burn zones). In addition to the nuclide reaction rates obtained from the flux solver, the depletion module requires decay constants for the nuclides and fission yields of the fission products. The energy released per fission and capture is a parameter that is also required for the depletion calculations. These parameters are generally obtained from the lattice code or from base cross section data sources like ENDF/B or JEF data libraries.

REBUS-3 Depletion and Fuel Cycle Analysis Code

The Argonne REBUS-3 code was developed for fast reactor depletion and fuel cycle analysis and hence does not have thermal feedback capability. However, it provides attractive features for thermal reactor calculations. The code contains a robust algorithm that permits the user to specify the burnup nuclides and the transmutation chains for the nuclides. There is no limit on the number of nuclides that can be represented. Ten reaction types are permitted by the code: (n,γ), (n,f), (n,p), (n,α), (n,2n), (n,d), (n,t), β- decay, β+ decay, and alpha decay. The solution of the transmutation and decay equations are obtained using the block depletion approach that permits the user flexible definition of planar and axial depletion zones. The code also allows the specification of burnup-dependent microscopic cross sections that are fitted with respect to a base isotope. This permits the accurate treatment of the nuclide self-shielding and neutron spectrum effects with burnup. The REBUS-3 code allows the user to select from a menu of different flux solvers. These include the DIF3D finite-difference and nodal diffusion theory solvers, and the VARIANT nodal transport solver. Additionally, the code can use the TWODANT module for calculating the neutron flux and power distribution.

The REBUS-3 code contains unique features not generally found in three-dimensional burnup codes. These include the ability to perform *equilibrium cycle* calculation in addition to the common non-equilibrium calculation. An external cycle capability is also provided by the code for modeling mass flows at the post-irradiation cooling, reprocessing, and fabrication stages

of the fuel cycle. For these cases, radioactive decay can be additionally modeled for specified time delays between various processes.

For the equilibrium (infinite repetition of periodic fuel management) type problems, the code uses specified external fuel supplies to load the reactor that is assumed operating under a fixed fuel management scheme. Optionally, reprocessing may be included in the specification of the external fuel cycle and discharged fuel may be recycled back into the reactor. For non-equilibrium (or explicit cycle-by-cycle) cases, the initial composition of the reactor core may be explicitly specified or the core may be loaded from external feeds, and discharged fuel may be recycled back into the reactor as in equilibrium problems. This second option permits modeling reactor operation under a specified periodic or non-periodic fuel management program. Four types of search procedures may be carried out in order to satisfy user-supplied constraints during fuel cycle calculations: (1) adjustment of the reactor burn cycle time to achieve a specified discharge burnup, (2) adjustment of the fresh fuel enrichment to achieve a specified multiplication constant at a specified point during the burn cycle, (3) adjustment of the control poison density to maintain a specified value of the multiplication constant throughout the reactor burn cycle, and (4) adjustment of the reactor burn cycle time to achieve a specified value of the eigenvalue at the end of the burn step.

DIF3D Eigenvalue and Flux Solver

The REBUS-3 code uses DIF3D or TWODANT as the flux and eigenvalue solver. The DIF3D module contains solution options for multigroup steady-state neutron diffusion and transport theory calculations. Cross section data provided in standard format (arbitrary group structure) are used in these calculations. Both nodal and finite-difference spatial discretization approaches are available in the code. Collectively, the nodal options solve the diffusion and transport equations in two- and three-dimensional hexagonal and Cartesian geometries. One-, two- and three-dimensional orthogonal (rectangular and cylindrical) and triangular geometry diffusion theory problems are solved by the DIF3D finite difference option. Eigenvalue, adjoint, fixed source and criticality search problems are permitted. Upscattering and internal black boundary conditions are also treated by the code. Solution for anisotropic scattering is available in the nodal transport solver VARIANT which uses the variational nodal transport method.

[7,10] The robust code editor allows flexible definition of edit regions and energy ranges. Flux and power density maps by mesh cell and region-wise balance integrals can be requested by the user.

Required Modifications to REBUS-3/DIF3D

Some code features that require development or upgrade in the REBUS-3/DIF3D code suite for VHTR analysis have been identified. These are:

1. Thermal calculation and feedback effect on cross sections: A thermal fluid capability is essential for realistic analysis and design of reactors. The production version of the REBUS-3/DIF3D does not have a thermal feedback option. Thermal effects are separately accounted for externally to the codes in fast reactor analysis, since a direct coupling in a neutronic code has been found unnecessary for quasi-static depletion analyses. Preliminary evaluations have indicated that this approach is insufficient for VHTR analysis [3] and consequently, a thermal feedback capability should be implemented in the REBUS-3 code.
2. Cross section representation accounting for energy and space self-shielding effects on all cross section types with burnup: Conceptually, since the cross sections of VHTR fuel elements vary significantly with burnup and fuel and moderator temperatures, a more generic capability than exists in the production version of REBUS-3/DIF3D is required to accurately represent these variations during whole-core depletion calculations.
3. Surface-dependent discontinuity factors: Advanced nodal diffusion methods typically employ nodal equivalence parameters (discontinuity factors) to reduce homogenization errors arising from core heterogeneity (different rodded and unrodded fuel and reflector regions, and interfaces between the regions). Surface-dependent discontinuity factors are particularly very useful to take into account geometric asymmetry in the nodal approach and thus must be provided.
4. Control rod simulation during depletion calculations: Since the control rod movement modeling capability currently available in the production version of REBUS-3 is not readily adaptable to VHTR control rod simulation, a new scheme is required.

5. Pin power reconstruction: Pin powers are recovered by imbedded local calculations or by superposition of global and local power distributions, which are respectively obtained from nodal and lattice calculations. Pin power factors generated from DRAGON calculations need to be implemented in DIF3D.

The pertinent modifications that have been made for the first four items are discussed in Section 3.0.

2.3 Interface Tool Between Lattice Physics and Whole-Core Codes

Cross section generation requires many DRAGON calculations for all components in the VHTR core of interest: fuel blocks with or without burnable poisons, radial and axial reflectors, and control rods. Anticipated output data from DRAGON calculations include discontinuity factors and pin power factors, along with ISOTXS-format files containing cross sections. With the DRAGON outputs, many data processing jobs are required to create the files necessary for REBUS-3/DIF3D calculations. Therefore, a toolkit named X-MANAGER (Cross-Section Manager) has been developed to help automate routine jobs and simplify data management. The X-MANAGER, programmed with the UNIX Shell and AWK commands, has the following major functions:

1. Run DRAGON depletion jobs for different temperature conditions.
2. Merge ISOTXS files into an ISOTAB file that has a hierarchical structure of isotope, burnup, and temperature; fission products can be lumped optionally; merge discontinuity factor and pin factor files into one file for each type.
3. Name cross sections with a unique composition index.
4. Run DRAGON and the finite difference method (FDM) code for a one-dimensional fuel-reflector model, and generate reflector cross sections adjusted by discontinuity factors.
5. Generate the macroscopic cross section changes due to control rod insertion from unrodded and rodded cross sections sets.
6. Read and print ISOTXS or ISOTAB files for debugging purposes.

Figure 1 displays the steps required to generate cross sections in DRAGON calculations, process them in the X-MANAGER, and use them in REBUS-3/DIF3D calculations. The cross

sections generated from DRAGON are adjusted using nodal equivalence parameters (simplified equivalence theory implementation) and merged into a single dataset for REBUS-3/DIF3D calculations. Using tabulated cross sections with respect to burnup and temperatures, REBUS-3/DIF3D performs whole-core calculations with thermal feedback and fuel depletion.

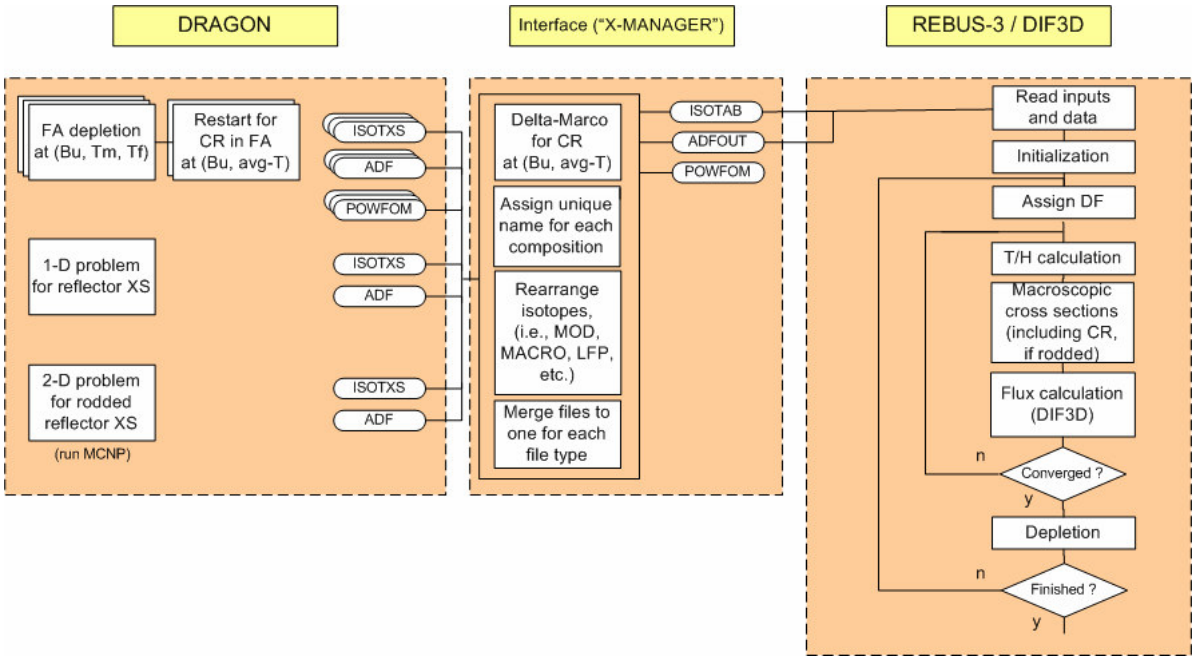

Figure 1. Data Flow for DRAGON, X-MANAGER, and REBUS-3/DIF3D.

3.0 MODIFICATIONS TO REBUS-3/DIF3D

3.1 Cross Section Module

Cross Section Representation

The current production version of REBUS-3/DIF3D obtains cross section data from a single ISOTXS file with a limited capability to represent the burnup dependency of cross sections and performs fuel cycle analysis as well as depletion calculations. This was quite adequate for fast reactor analysis since the coupling between neutronic and thermal-fluid calculations could be de-coupled in static calculations, without significant loss in accuracy; the coupling is done outside the neutronic code. For thermal reactors, however, neutron cross sections change significantly with state parameters. Additionally, the spectrum of a fuel or reflector element could impact locally that of the neighboring element. Therefore, to accurately estimate core fluxes, powers, and reactivities it is necessary to implement a more general capability. Thus, cross sections need to be functionalized or tabulated against state parameters such as burnup, fuel and moderator temperatures, etc., so that cores with various conditions can be modeled with reasonable accuracy.

The tabulation approach is the simplest and most stable form for cross section representation. It however requires a relatively large amount of data points to give the required accuracy. Cross section functionalization is typically more efficient than the tabulation approach because it could cover a wide range of data points with a combination of functions, but it requires effort to functionalize the data and may incur a loss of accuracy in estimating data, even within the range. Therefore, it was initially decided to use the tabulation approach for cross section representation.

The DRAGON code generates cross section files in an ISOTXS format at various conditions for a given core design. The ISOTXS files for the different states (burnup and temperature) are merged into one file named ISOTAB, for use by the REBUS-3/DIF3D code. Rather than a simple concatenation of multiple files, this process is a restructuring of the ISOTXS data into that shown in Figure 2, such that cross sections are systematically sorted with state parameters. In ISOTAB, cross section data is categorized in turn by isotope, burnup, and temperature. If a new state parameter is introduced, it would be placed inside the burnup loop.

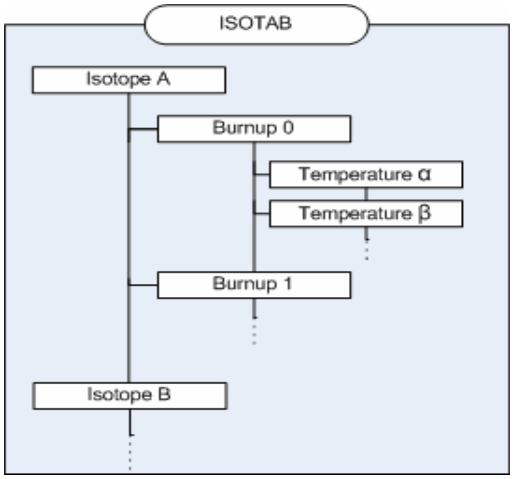

Figure 2. Structure of ISOTAB File.

Currently, an ISOTAB file is able to handle many isotopes with designated names or prefixes. The pertinent isotopes of the elements shown in Table 1 have been represented. The number of isotopes represented is quite adequate to capture core reactivity effects, but can easily be increased. Of the fission products, eight isotopes are always treated independently even when fission products are chosen to be lumped. The fixed isotopes, MOD, LFP, DUMP, MACRO, and CROD, are created although they are not defined in the DRAGON input.

Table 1. Isotope Indices of ISOTAB.

Type	Isotope Index
Fixed Name*	MOD, LFP, DUMP, MACRO, CROD
Fission Products (Always separate)	XE (135), I (135), SM (149), PM (147, 147m, 148, 148m, 149)
Fission Products (Lumped optionally)	EU, SM, ND, CS, XE, I, PD, RH, RU, TC, KR, MO, CD, IN, GD, AG, EU
Burnable Poison	B, ER
Actinide	TH, PA, NP, U, PU, CM, AM
Others	HE, GRA, O, FE, C, SI, AL

* MOD : Macroscopic cross section for moderator
LFP : Effective microscopic cross section for lumped fission product
DUMP : Macroscopic cross section for undefined isotopes
MACRO : Total macroscopic cross section
CROD : Delta macroscopic cross section for control rod

To handle the ISOTAB file in REBUS-3, new modules such as NEUTRONXS, COMPACTSCAT, and GENERALISOTOPE have been developed using FORTRAN 90/95 object-oriented data structures. The NEUTRONXS module provides a new cross section storage procedure, while the GENERALISOTOPE module constructs a complete set of microscopic cross section data for all isotopes. The COMPACTSCAT module contains a single block of banded scattering data which allows a reduced memory usage and an easy data transfer from and to disk. Additionally, the DIFFERENTIALBURNUP routine has been developed to obtain material- and stage-dependent burnups for use in the calculation of burnup-dependent cross sections.

Depletion with Explicit or Lumped Fission Product Model

The 69-group and 172-group WIMSD4-format cross section libraries created at Argonne have been used with the DRAGON code in this work. In order to reproduce the nuclide number densities of DRAGON depletion calculations for a single fuel block in REBUS-3 calculations, the depletion chains in both codes should be consistent. The DRAGON cross section libraries used in this work have 38 fission products, which results in a large amount of data in a single cross section file, and large memory and computing time requirements in REBUS-3 whole-core depletion calculations. Consequently, a code option has been provided to merge and treat fission products as a single lumped fission product in order to save space, memory, and computing time in REBUS-3 calculations. However, even in the case of using the lumped fission product, specific fission products such as I-135, Xe-135, Pm-147, Pm-147m, Pm-148, Pm-148m, Pm-149, and Sm-149 are traced explicitly because they have relatively short half-lives and large absorption cross sections that change with core flux levels.

To generate the cross sections for the lumped fission product, the number density of the lumped fission product (LFP) is set to the sum of the number densities for the fission products that are merged and the fission product cross sections are averaged by weighting with their number densities. Fission product yields from actinides are simply added up. For a given actinide, the depletion equation for a lumped fission product is as follows:

$$\frac{dN_{LFP}}{dt} = \gamma_{LFP}\Sigma_f\phi - N_{LFP}\sigma_{LFP}\phi, \qquad (1)$$

where $N_{LFP} = \sum_{i \in LFP} N_i$, $\sigma_{LFP} = \left(\sum_{i \in LFP} N_i \sigma_i \right) / N_{LFP}$, $\gamma_{LFP} = \sum_{i \in LFP} \gamma_i$.

The depletion results for a single fuel block obtained using REBUS-3 with the explicit and lumped fission product models have been compared to those from the DRAGON code. To minimize deviations arising from different depletion methods and flux solutions employed in the codes, the DRAGON depletion was performed with an infinite spectrum option, and both DRAGON and REBUS-3 used a small time step (2 days). Figure 3 shows that both the REBUS-3 explicit and lumped fission depletion models give results that are in very good agreement with DRAGON results.

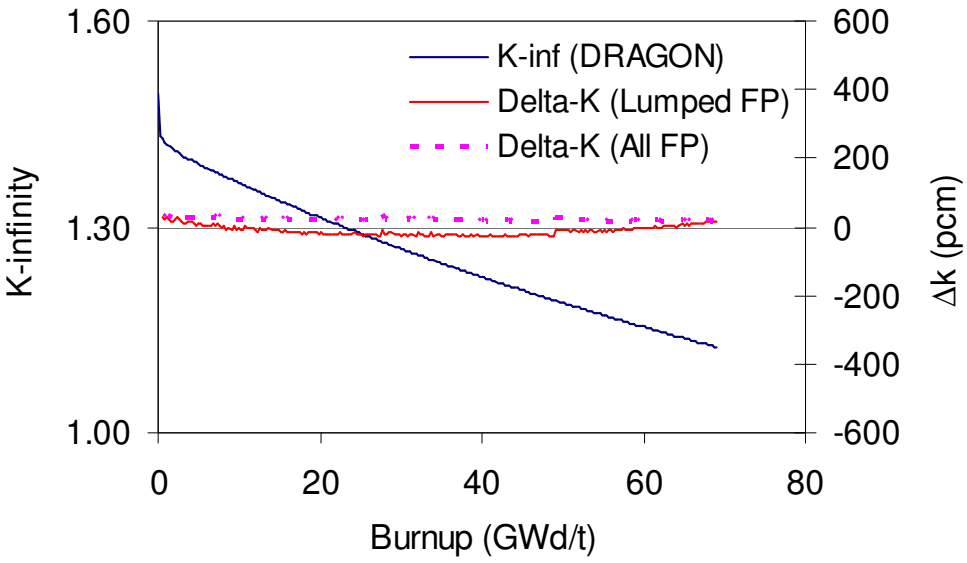

Figure 3. Comparison of k-infinity Values from DRAGON and REBUS-3 with Burnup.

3.2 Simplified Thermal-Hydraulic Feedback Module

A simple heat conduction model has been incorporated into the DIF3D code to compute the average temperatures of the graphite block and fuel compact. In order to examine the importance of axial conduction, the radial and axial temperature gradients have been compared for the average and high power locations of the GT-MHR design, which is similar to the

VHTR/NGNP design with respect to heat conduction. [1, 2] The estimated temperature gradients in the graphite block and fuel compact are summarized in Table 2. It can be seen that each axial temperature gradient is less than 1.5% of the corresponding radial gradient. Thus, the axial conduction term can be neglected without introducing a significant error.

A planar temperature distribution model for VHTR cores was established based on the unit cell shown in Figure 4. Using the computational fluid dynamics code STAR-CD [11], two-dimensional heat conduction equations were solved for various heat generation rates and heat conduction coefficients. Figure 5 shows an example planar distribution of a unit cell temperature, and Figure 6 shows an example temperature distribution for a 1/6-th core.

Table 2. Typical Temperature Gradients of GT-MHR Design.

Location		Fuel Compact		Graphite	
		Axial (ºC/cm)	Radial (ºC/cm)	Axial (ºC/cm)	Radial (ºC/cm)
Average Power	Mid-height	0.59	63	0.59	48
	Bottom	0.32	30	0.32	20
High Power	Mid-height	0.88	87	0.91	65
	Bottom	0.38	47	0.44	33

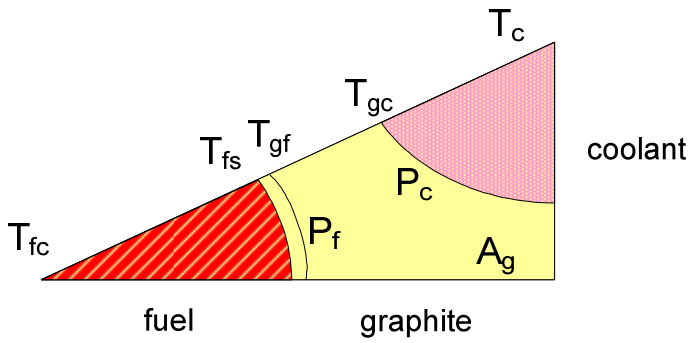

Figure 4. Thermal-Hydraulic Unit Cell Model of VHTR.

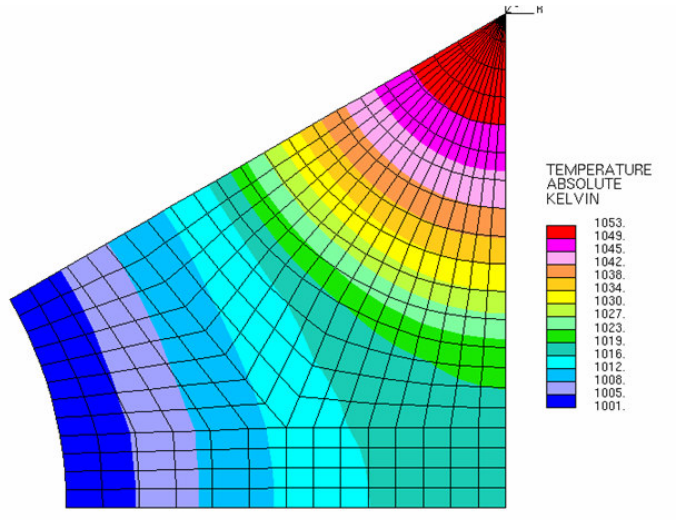

Figure 5. Planar Temperature Distribution in Unit Cell of GT-MHR.

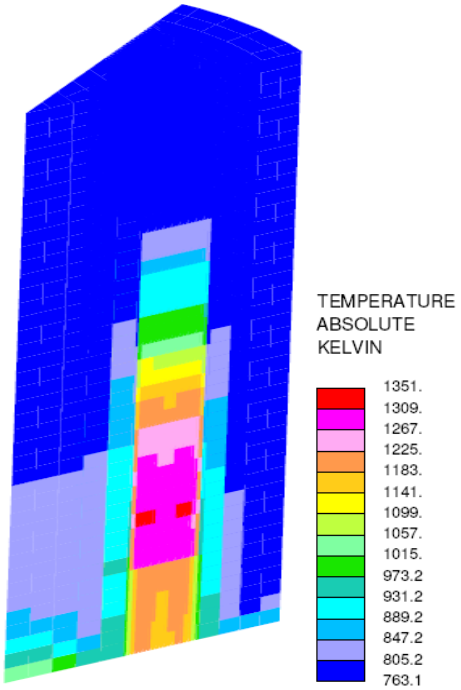

Figure 6. Axial Temperature Distribution of GT-MHR.

Based on the planar temperature distribution, it was found that the temperatures of the graphite-coolant interface (T_{gc}), graphite-fuel interface (T_{gf}), fuel surface (T_{fs}), and the fuel centerline temperature (T_{fc}) could be approximately determined with the following simple formulas:

$$T_{gc} = T_c + \frac{q_s''}{h_c}, \tag{2}$$

$$T_{gf} = T_{gc} + \frac{2A_g}{P_f + P_c}\frac{q_s''}{k_g},$$

$$T_{fs} = T_{gf} + \frac{q_s''}{h_g},$$

$$T_{fc} = T_{fs} + \frac{r_f}{2}\frac{q_s''}{k_f},$$

where q_s'' = Heat flux at the fuel surface,

T_c = Bulk coolant temperature,

h_c, h_g = Heat transfer coefficient at coolant hole surface and fuel compact gap,

r_f = Radius of fuel compact,

A_g = Area of graphite block of the unit cell model,

P_f, P_c = Arc length of fuel compact and coolant channel of the unit cell model,

k_f, k_g = Heat conduction coefficient of fuel compact and graphite block.

The average fuel and graphite temperatures used for the temperature feedback calculation can be determined as weighted averages of T_{fc}, T_{fs}, T_{gc}, and T_{gf} as:

$$\overline{T}_f = (1 - w_f)T_{fc} + w_f T_{fs}, \tag{3}$$

$$\overline{T}_g = (1 - w_g)T_{gc} + w_g T_{gf},$$

where T_{fc} = Fuel centerline temperature,

T_{fs} = Fuel surface temperature,

T_{gf} = Graphite temperature at the interface with fuel,

T_{gc} = Graphite temperature at the interface with coolant,

w_f = 0.66, $w_g = 0.61$.

It was found that compared to STAR-CD results, these formulas compute the average fuel and graphite temperatures within 1 ºC error.

For a gas coolant, the pressure is required to determine the heat transfer coefficient since the conductivity depends on the pressure. However, the pressure calculation is complicated to be incorporated in the thermal-hydraulic feedback calculation for steady-state analyses. Therefore, the possibility of estimating the heat transfer coefficients with a constant pressure was investigated. Table 3 shows the coolant properties and heat transfer coefficients at the core inlet and outlet estimated for the GT-MHR design. The pressure drop over the core with 793 cm high is only 0.05 MPa (0.7% of operating pressure), and hence the heat transfer coefficient varies by only 4.4%. This variation of heat transfer coefficient would lead to a variation less than 2 ºC in the temperature difference between the graphite surface temperature and the bulk coolant temperature, since its maximum difference is ~75 ºC at the core mid-height. As a result, for the steady-state thermal hydraulic feedback calculation, the pressure variation along the coolant channel can be neglected.

Table 3. Typical Heat Transfer Coefficients at Core Inlet and Outlet of GT-MHR Design.

Parameter	Inlet	Outlet
Hydraulic diameter (m)	1.59E-02	1.59E-02
Coolant mass flux (kg/m^2-s)	112.15	112.15
Pressure (MPa)	7.07	7.02
Temperature (ºC)	491	850
Density (kg/m^3)	2.23	1.50
Velocity (m/s)	50.39	74.59
Viscosity (Pa·s)	3.849E-05	5.04E-05
Specific heat (kJ/kg-K)	5.202	5.202
Thermal conductivity (W/m·s)	0.301	0.387
Reynold number	46251	35322
Prandtl number	0.665	0.677
Peclet number	30769	23913
Nusselt number	105	85.59
Heat transfer coefficient (W/m^2·s)	1999	2088

Change of conductivities of fuel compact and graphite with temperature is not negligible. Thus, fuel compact and graphite conductivities are implemented as a function of temperature as shown in Equation (4):

$$k_f\,[W/mK] = 0.0036 \cdot T + 3.9429, \qquad \text{T} \in [220\text{ K}, 2200\text{ K}] \tag{4}$$

$$k_g\,[W/mK] = -1.319\times10^{-8} \cdot T^3 + 4.733\times10^{-5} \cdot T^2 - 3.939\times10^{-2} \cdot T + 36.25,$$

To implement the thermal-fluid function in REBUS-3, the HMG4C module has been changed and the SIMPTH module has been added. The HMG4C module reads the binary files GEODST, LABELS, NDXSRF, ZNATDN, DLAYXS, and ISOTXS, and produces the COMPXS file, which contains macroscopic cross sections to be used in DIF3D calculations. The NEUTRONXS module which has been developed for the cross section tabulation approach is used to obtain cross sections of corresponding compositions for given burnup and temperatures. The SIMPTH module solves the thermal conduction equation for each unit cell, based on the input data for thermal calculations. To allow the input for thermal calculations, a new input file, A.THERM, has been defined. Figure 7 shows the execution flows of the two modules.

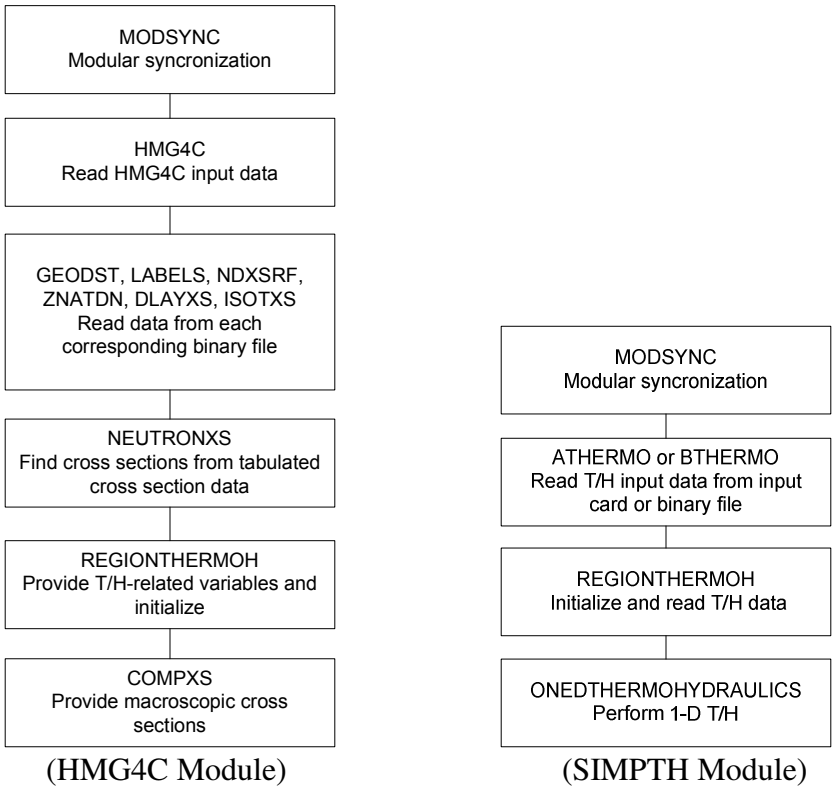

Figure 7. Execution Flow of HMG4C and SIMPTH Modules.

The original DIF3D calculation path has been modified to incorporate the SIMPTH module. Figure 8 illustrates a modified sequence for the DIF3D driver. The new sequence includes first performing thermal-fluid calculation using the ONEDTHERMOHYDRAULICS routine of SIMPTH, and then adjusting the cross sections to reflect the thermal states. The code then proceeds to calculate the core multiplication factor and flux distribution. This sequence is repeated until the flux distribution is converged.

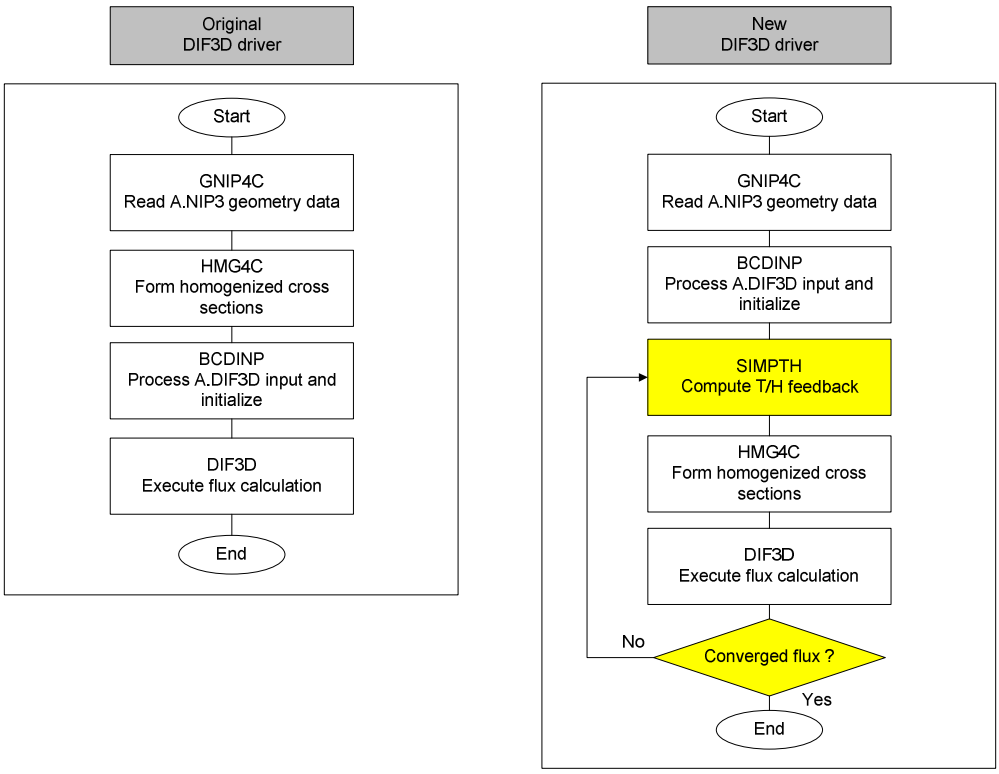

Figure 8. Execution Flow of Modified DIF3D Driver.

3.3 Control Rod Module

The control rod movement model in the production version of REBUS-3 moves the whole assembly, since typical sodium-cooled fast reactors employ separate control assemblies from fuel assemblies. This model is inadequate for VHTR designs in which the control rods are moving through the designated holes in fuel and reflector blocks. To support this VHTR design feature, new routines have been written in REBUS-3 to simulate the pertinent control rod motion. New input cards have been defined in A.THERM for control rod location, composition, axial steps of each control rod bank as a function of burnup, etc. In addition, the ATHERMO and

FILL_IN_COMPXS modules have been updated, as shown in Figure 9, such that macroscopic cross sections of rodded nodes are updated with control rod cross sections before DIF3D calculations.

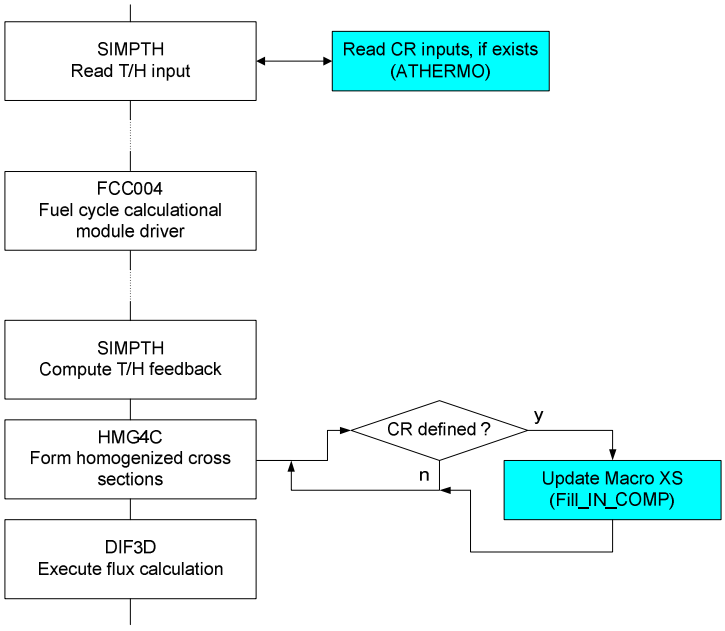

Figure 9. Application of Delta-Macroscopic Cross Sections of Control Rod in REBUS-3.

This new function requires definition of a separate region for each fuel assembly and each reflector region with a control rod, so that control rod cross sections are smeared only in the fuel assembly and reflector region of concern. For this, control rod cross sections are represented as delta macro cross sections:

$$\Delta\Sigma_{\alpha g} = \Sigma_{\alpha g}^{rodded} - \Sigma_{\alpha g}^{unrodded}, \tag{5}$$

where g = group, α = cross section type.

3.4 Surface-Dependent Discontinuity Factors

Discontinuity factors (DFs) based on the nodal equivalence theory were implemented within the hexagonal diffusion option of the DIF3D code in 1992. [12, 13] The implementation was focused on fast reactor system analysis, and thus introduced sets of group-dependent discontinuity factors for the surface flux (f_α), partial currents (g_α^i, g_α^o), and flux moment (m_α),

where $\alpha \in \{x,u,v,z\}$ and superscripts i and o denote incoming and outgoing directions, respectively. The weighed quantities for surface flux ($\tilde{\phi}_\alpha / f_\alpha$), incoming and outgoing partial currents ($\tilde{J}^i_\alpha / g^i_\alpha$ and $\tilde{J}^o_\alpha / g^o_\alpha$), and moments ($\tilde{M}_\alpha / m_\alpha$) allow conserving the reference eigenvalue, node-average fluxes and surface currents. Thus, 28 discontinuity factors per group are prepared for 3-D hexagonal cells, which include 8 surface flux, 8 outgoing current, 8 incoming current, and 4 moment discontinuity factors.

The discontinuity factor scheme described above has now been simplified such that only surface flux discontinuity factors (f_α) are used, in the same way as applied to thermal reactor analysis (e.g., LWRs). Discontinuity factors are generated on a single fuel assembly basis, comparing surface-average and assembly-average fluxes.

The main part of DIF3D influenced by the discontinuity factors is the partial current-based response matrix equation:

$$\mathbf{J}_g^{out} = \mathbf{R}_g \mathbf{J}_g^{in} + \mathbf{P}_g \mathbf{Q}_g , \tag{6}$$

where $\mathbf{J}_g^{out}$ = Outgoing current vector for group g,

$\mathbf{J}_g^{in}$ = Incoming current vector for group g,

$\mathbf{R}_g$ = Response matrix for group g,

$\mathbf{P}_g$ = Source response matrix for group g,

$\mathbf{Q}_g$ = Source moment vector for group g.

A simple transformation can be made before and after solving for the response matrix to apply the discontinuity factor:

$$A J_g^{het} = J_g^{\hom}, \tag{7}$$
$$A^{-1} J_g^{\hom} = J_g^{het},$$

where J_g^{het} = Heterogeneous partial current vector for group g,

J_g^{hom} = Homogeneous partial current vector for group g,

$$A = \begin{bmatrix} \alpha & \alpha - 1 \\ \alpha - 1 & \alpha \end{bmatrix},\ \alpha = \frac{f_g + 1}{2 f_g},\ f_g = \frac{\phi_g^{het}}{\phi_g^{\text{hom}}}.$$

Instead of saving homogeneous partial currents, heterogeneous ones are saved in memory, and homogeneous partial currents are estimated on the fly before solving the response matrix whose solutions are converted and saved back into the heterogeneous ones. The additional change would be the definition of homogeneous surface fluxes based on heterogeneous partial currents as:

$$\phi_{gs}^{\text{hom}} = \left(j_{gs}^{out,het} + j_{gs}^{in,het} \right) / f_{gs} \tag{8}$$

where ϕ_{gs}^{hom} = Homogeneous surface flux for group g, surface s,

$j_{gs}^{out,het}$, $j_{gs}^{in,het}$ = Heterogeneous outgoing and incoming partial currents, respectively, for group g, surface s.

f_{gs} = Discontinuity factor for group g, surface s.

Due to the simplicity of the transformation, only the routines associated with the response matrix algorithm need to be changed. Since, however, DIF3D uses incoming partial currents and surface fluxes as intermediate terms to calculate coefficients and moments, several routines have to be additionally modified. In order to minimize changes, the modified routines utilize the same discontinuity factor variables and dimensions as used for the previous scheme. Thus, the unused discontinuity factor arrays such as incoming, outgoing, and moment factors (g_α^i, g_α^o, m_α) are set to unity so that they do not affect the code solution.

The DIF3D code reads discontinuity factors for core zones from the DISFAC file (binary format) which is converted from the ADISFAC file (ASCII format). Since it is assumed that discontinuity factors are not affected by temperature change, they are updated only with burnup. For format conversion, the WRITEDF routine has been developed, which is called during depletion calculations as shown in Figure 10. Currently, format conversion is carried out manually outside the code system, but should be integrated into the REBUS-3 code in the future.

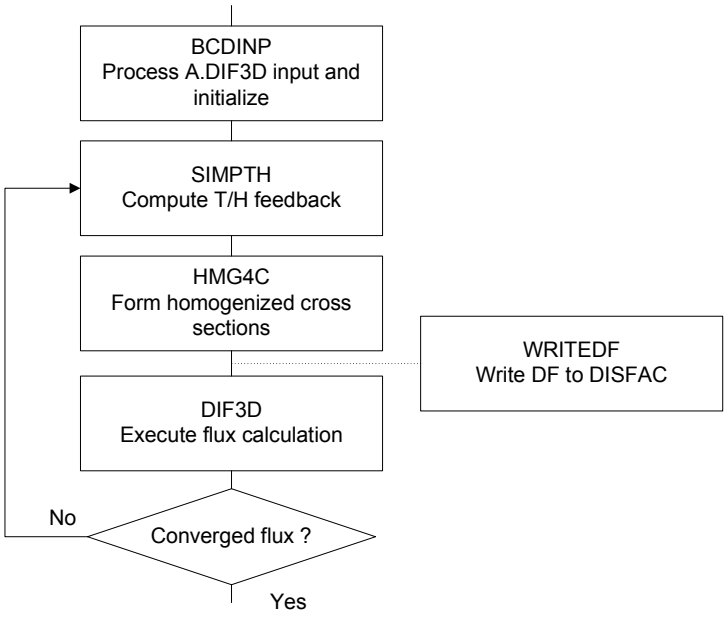

Figure 10. Application of Surface-Dependent Discontinuity Factors to DIF3D.

Several routines listed in Table 4 have been changed for modification of the previous discontinuity factor scheme. Most of them are routines computing partial currents and surface average fluxes.

Table 4. Routines Associated with Surface-Dependent Discontinuity Factors.

Routine	Description
PCHEX	Convert xy-plane homogeneous and heterogeneous partial currents based on Eq. (7)
PCZ	Convert z-directional homogeneous and heterogeneous partial currents based on Eq. (7)
SRCHEX	Calculate xy-plane homogeneous partial currents based on Eq. (7) for source term
SRCZ1	Calculate z-directional homogeneous partial currents based on Eq. (7) for source term
FLXHEX	Compute xy-plane surface fluxes based on Eq. (8) for flux moments
FLXZ	Compute z-directional surface fluxes based on Eq. (8) for flux moments
DFINIT	Initialize discontinuity factor arrays by setting partial current and moment factors to unity

4.0 VERIFICATION

Two-dimensional (2-D) and three-dimensional (3-D) VHTR core calculations have been performed using the REBUS-3/DIF3D/DRAGON code suite. Fuel block specifications for the cores are the same as those defined in Reference 8. The fuel form is uranium oxy-carbide ($UC_{0.5}O_{1.5}$) and the fuel element has 216 fuel holes and 108 coolant holes. The pitch of the coolant hole or fuel compact is 1.8796 cm and the radii of the fuel compact and fuel holes are 0.6223 and 0.635 cm, respectively. There are 102 large coolant holes with radius of 0.794 cm and 6 small coolant holes with radius of 0.635 cm. Burnable poison (BP) rods consist of B_4C granules dispersed in graphite compacts and are loaded at the six corners of the hexagonal block. A control rod is located in one 1/6-sector of a fuel or reflector block. The control rod material consists of 40 w/o enriched boron (90% B-10), contained in B_4C granules dispersed uniformly in a graphite matrix and formed into annular compacts. The core power level is 600 MWt with a power density of 6.6 MW/m^3. The whole core is composed of 11-ring hexagonal columns: the active core has 102 fuel columns that are located in rings 6, 7, and 8. Ten graphite fuel blocks (elements) stacked vertically comprise a fuel column with an active core height of 793 cm.

The DRAGON code has been run for the VHTR fuel element ($UC_{0.5}O_{1.5}$) described above at 300 K, and its results were compared with those from the MCNP code. Both MCNP and DRAGON libraries are based on ENDF/B-VI nuclear data. Table 5 indicates that the MCNP and DRAGON results agree well within 0.14% $\Delta\rho$ when the homogeneous fuel compact model is used; the double heterogeneity effect is ~3.5% $\Delta\rho$ and it is overestimated in DRAGON calculations by ~0.5% $\Delta\rho$. Thus, the homogeneous fuel compact model is used predominantly in

Table 5. Comparisons of k_{inf} from MCNP and DRAGON for Fuel Element ($UC_{0.5}O_{1.5}$).

Fuel Compact Model	Fuel Block	k_{inf}		% $\Delta\rho$
		MCNP	DRAGON	
Homogeneous Fuel Compact	No BP	1.47433 (±0.00027)	1.47522	0.041
	BP	1.20780 (±0.00031)	1.20982	0.138
Explicit TRISO Particles	No BP	1.52908 (±0.00030)	1.54061	0.490
	BP	1.25252 (±0.00022)	1.26129	0.555

subsequent verification tests in order to minimize errors arising from the deterministic lattice code itself. Also, fuel compacts with explicit TRISO particle representation are used in benchmark calculations since they are the actual fuel configuration in VHTR cores.

4.1 Cross Section Generation

Fuel Block Cross Sections

Fuel block cross sections are generated using single block calculations with reflective boundary conditions, assuming that the neutron spectrum of the fuel block is primarily dependent on its own characteristics (i.e., not influenced by neighboring blocks). Due to the geometric limitation of the DRAGON code, the fuel-element handling hole in the center of the fuel block is approximated using two-ring hexagonal cells with the number density of graphite modified to preserve the graphite content of the fuel block; a jagged boundary thus results instead of the actual circular boundary. Recall that the fuel block boundary is also jagged because of the lack of a model with flat boundary. Thus, to derive nodal equivalence-theory-based discontinuity factors with the jagged boundaries, small circular regions are defined at the centers of the peripheral hexagonal cells and then surface averaged fluxes are estimated using the fluxes in those circular regions. This approximation will be replaced when flat boundaries are implemented in DRAGON in the future.

The adequacy of approaches used for generating fuel block cross sections and equivalence parameters has been tested with the following four cases using a two-ring (seven-block) core model:

- Case BP-1: A BP loaded fuel block is located at the center of the model,
- Case BP-2: A BP loaded fuel block is located on the periphery of the model,
- Case CR-1: A control rod loaded fuel block is located at the center of the model,
- Case CR-2: A control rod loaded fuel block is located on the periphery of the model,

For cases CR-1 and CR-2 the control rod is located at the center of the fuel block (model avoids the difficulty of the asymmetrically loaded control rod in the actual design). As can be seen in Table 6, the application of discontinuity factors (DFs) reduces the multiplication factor errors by

70 ~ 100 pcm for BP loaded cores and 500 ~ 800 pcm for control rod loaded cores. In addition, the maximum power errors are significantly reduced, especially for the cores with control rod.

Table 6. Performance of Discontinuity Factors for 2-D Mini-Core Models with BP or CR.

Core	Code			k_{eff}	% Δρ	Max % Power Err.
BP loaded Core	Case BP-1	MCNP		1.42957 (±0.00029)	-	-
		DRAGON/ DIF3D	w/o DF	1.43400	0.310	-3.2
			w/ DF	1.43258	0.211	0.3
	Case BP-2	MCNP		1.43467 (±0.00028)	-	-
		DRAGON/ DIF3D	w/o DF	1.43715	0.173	-1.8
			w/ DF	1.43613	0.102	1.0
CR loaded Core	Case CR-1	MCNP		1.33365 (±0.00031)	-	-
		DRAGON/ DIF3D	w/o DF	1.31701	-1.248	11.2
			w/ DF	1.32753	-0.459	1.3
	Case CR-2	MCNP		1.36702 (±0.00030)	-	-
		DRAGON/ DIF3D	w/o DF	1.35419	-0.938	11.2
			w/ DF	1.36051	-0.477	3.6

Figures 11 and 12 are comparisons of the power distributions from MCNP and DIF3D calculations for the BP and CR cases, respectively. It is observed in Case BP-2 that power errors are over-corrected by discontinuity factors. This suggests that discontinuity factors derived from a single block model may not be accurate in some cases. This can be improved by introducing current-based discontinuity factors in the future, which can account for the change in discontinuity factors with the actual boundary condition.

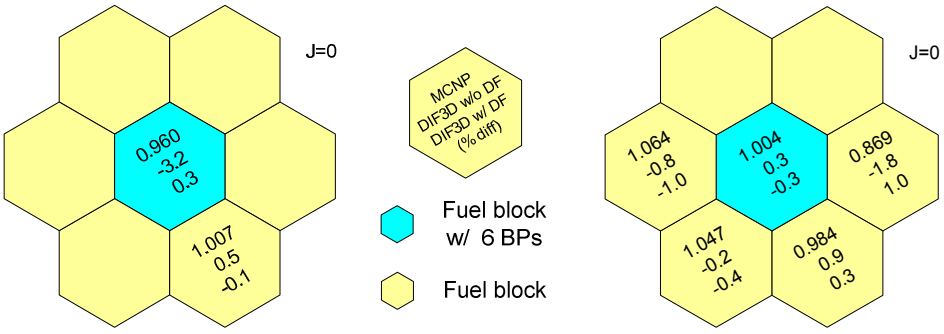

(Case BP-1) (Case BP-2)

Figure 11. Results of 2-D Mini-Core Models with Burnable Poison Loaded Fuel Block.

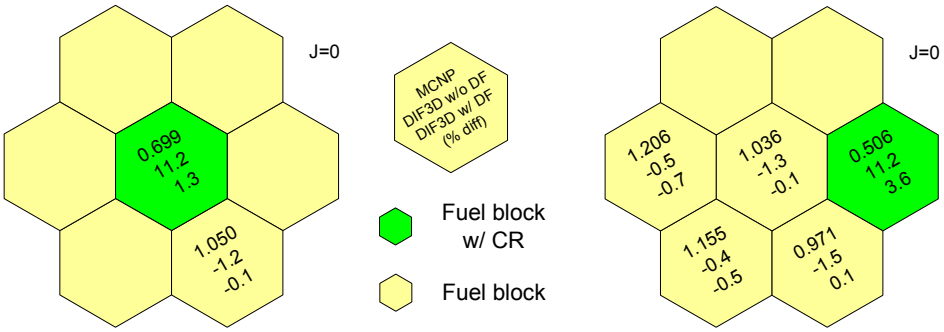

(Case CR-1) (Case CR-2)

Figure 12. Results of 2-D Mini-Core Models with Control Rod Loaded Fuel Block.

Reflector Cross Sections

Few-group reflector cross sections vary significantly with distance from the interface between the core and reflector regions because the thermal neutron spectrum changes significantly at this interface. The application of discontinuity factors makes it possible to use a single-set of cross sections for each of the inner, outer, and axial reflector regions with good accuracy. A two-region (fuel-reflector) one-dimensional model is used to generate the reflector cross sections. Discontinuity factors at the interface between the fuel and reflector are calculated by comparing the homogenous surface fluxes obtained from a finite difference method (FDM) solution and the heterogeneous surface fluxes of the DRAGON solution. [8]

Cross Sections for Reflector Region with Control Rod

For generating cross sections for a reflector region containing control rod, two approaches have been considered. In the first approach, a 1-D fuel-reflector model corresponding to a 2-D seven-block model is used to determine the control rod position in the 1-D reflector region iteratively such that the control rod worth determined by the model is sufficiently close to that of the reference 2-D solutions; the MCNP code is currently used for the 2-D (color-set) calculations, because the DRAGON code does not properly support a multi-block model. [8] This approach is advantageous because of its simplicity, but it does not provide surface-dependent discontinuity factors. Consequently, it does not accurately capture the power tilt due to asymmetric loading of control rods.

It has been observed that the application of surface-dependent discontinuity factors is required for accuracy when a block is not symmetric (e.g., rodded reflector or fuel blocks). Thus, a second approach was investigated. In this approach, region-wise average fluxes, surface fluxes, and currents are derived from MCNP solutions. The MCNP region-wise flux data are imported into DRAGON to calculate homogenized cross sections for the rodded reflector block. The surface fluxes and currents from the MCNP calculation are employed to calculate discontinuity factors at the six surfaces of the rodded reflector block. [8] This latter approach, using surface-dependent discontinuity factors, was found to reduce the error in fuel block powers significantly.

In this study, cross sections are generated for two types of control rod configurations: (1) a rodded reflector block surrounded by 3 fuel and 3 reflector blocks (Type A) and (2) a rodded block surrounded by 2 fuel and 4 reflector blocks (Type B), which are discussed in details in Reference 8. Figure 13 illustrates these reflector block types.

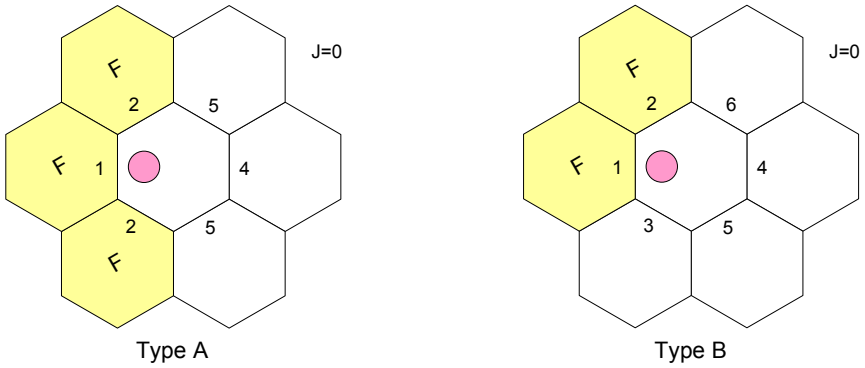

Figure 13. Two-Dimensional Modeling for the Rodded Reflector Region.

4.2 Two-Dimensional Calculations

Cores with or without Burnable Poisons

Two-dimensional core problems have been developed for the verification of the code suite. The radial layouts of these cores are illustrated in Figure 14. In the first core model (uniform core), fuel blocks of one type are loaded in the active core (annular) zone. These fuel blocks have no burnable poison or control rod material. In the other model (core with BP), the active core contains 30 BP-loaded fuel blocks. Using DRAGON, fuel block cross sections were generated from single fuel block calculations and the reflector cross sections were determined from the 1-D fuel-reflector model discussed in the previous section. Discontinuity factors are

applied to the cross sections using the simplified equivalence theory (SET) approach, [14] instead of employing surface-dependent values.

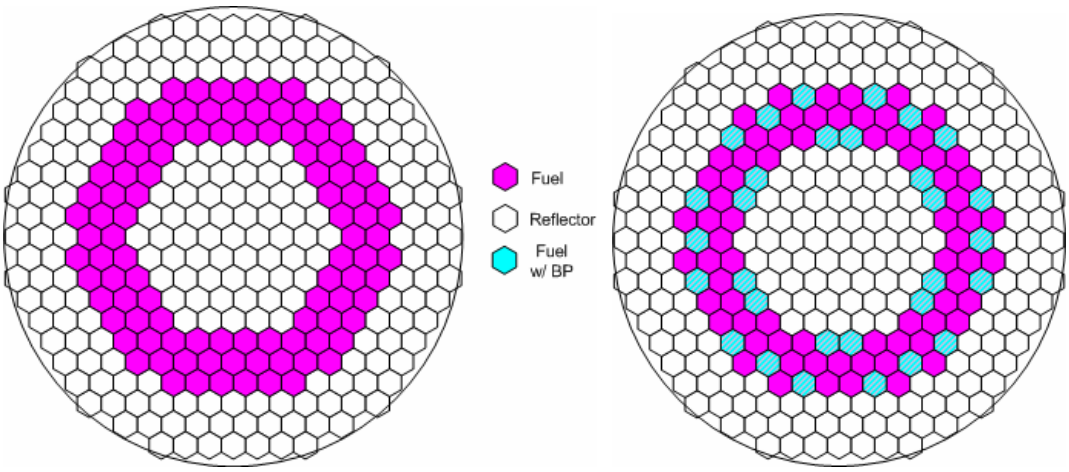

Figure 14. Two-Dimensional Core Configurations with and without Burnable Poisons.

Different DIF3D calculations have been performed for the uniform 2-D core using three Hex-Z/Tri-Z solution options in order to compare solution accuracy. The Hex-Z nodal diffusion theory (DIF3D-nodal), Hex-Z nodal transport theory (DIF3D-VARIANT) and Tri-Z finite difference diffusion theory (DI3D-FD) options of the code were used for this purpose. Note that the diffusion approximation of the DIF3D-VARIANT option was used in this study to evaluate its superior spatial approximations compared to the DIF3D-nodal option. Since the purpose of the current work is to study the solution accuracy, cross sections are generated using the homogeneous fuel compact model. The DIF3D-nodal calculation was performed using fourth-order flux approximation and constant transverse leakage approximation for each half hexagon in the plane. The DIF3D-VARIANT calculation was done using sixth-order source and flux approximations with the linear leakage approximation. The DIF3D-FD calculations were performed using 864 triangular meshes per hexagonal block (equivalent to 12 triangles per side).

Results from the DIF3D calculations have been compared to those from a reference MCNP calculation and are summarized in Table 7. The multiplication factors (k_{eff}) predicted by the DIF3D-VARIANT and DIF3D-FD options and MCNP are quite similar. The difference between the MCNP and the DIF3D-nodal solutions is slightly higher (0.4 - 0.7% $\Delta\rho$). The lower accuracy of the DIF3D-nodal option is attributed to the relatively poor approximation for the

transverse leakage in the plane; a constant leakage approximation for each half hexagon is employed. The core power distributions predicted by the nodal options are sufficiently accurate compared to the MCNP distribution (highest root-mean-square [RMS] difference in assembly powers of 1.3% and the maximum assembly power difference of 2.6%). The results also show the superior accuracy of the DIF3D-VARIANT option compared to the DIF3D-nodal option. While the DIF3D-FD solution is quite acceptable, it however requires a larger run-time storage container and longer computation time than the nodal options.

Table 7. Accuracy of Hex-Z/Tri-Z Solution Options of DIF3D.

Fuel Compact Model	Code		k_{eff}	% Δρ	Power Error (%)	
					RMS	Max
Homogeneous Fuel Compact	MCNP		1.39689 (±0.00032)	-	-	-
	DRAGON/ DIF3D* (w/o DF)	VARIANT	1.39852	0.083	1.3	2.6
		Nodal	1.38916	-0.398	1.2	2.2
		FDM	1.39773	0.045	-	-
	DRAGON/ DIF3D* (w/ DF)	VARIANT	1.39223	-0.240	0.8	1.3
		Nodal	1.38304	-0.717	0.9	1.7
		FDM	1.39156	-0.286	-	-

* 23 group cross sections used for DRAGON/DIF3D calculations.

More detailed comparisons of the results for the uniform core are presented in Table 8. The DIF3D-VARIANT results are shown along with the reference MCNP results; DIF3D results were obtained using 23-group and 172-group calculations. Results with homogeneous and explicit compact models for generating cross sections are also presented.

The two MCNP results show that the double heterogeneity effect is ~2% Δρ at the core level, which indicates the need to have a lattice model that accurately treats this effect. All the multiplication factors obtained from the DRAGON/DIF3D calculations agree reasonably well with the MCNP results. It is noted that using discontinuity factors reduces the maximum power errors by 0.6 ~ 1.3%. Additionally, the maximum power errors occur at the fuel block positions adjacent to outer reflector regions. The application of discontinuity factors lowers the k_{eff} by 0.20 to 0.32% Δρ, which is closer to the MCNP solution for the core model with explicit TRISO particle representation, but results in over-correction for the core with homogeneous fuel compacts. The results of power distribution comparisons are presented in Figures 15 and 16.

Table 8. Comparison of k_{eff} and Power for 2-D Core Models without BP or CR.

Fuel Compact Model	Code			k_{eff}	%Δρ	Power Error (%)	
						RMS	Max
Homogeneous Fuel Compact	MCNP			1.39689 (±0.00032)	-	-	-
	DRAGON /DIF3D*	w/o DF	172g	1.39567	-0.063	1.7	3.2
			23g	1.39852	0.083	1.3	2.6
		w/ DF	172g	1.39128	-0.289	1.2	2.4
			23g	1.39223	-0.240	0.8	1.3
Explicit TRISO Particles	MCNP			1.43610 (±0.00021)	-	-	-
	DRAGON /DIF3D*	w/o DF	172g	1.44054	0.215	2.2	1.4
			23g	1.44346	0.335	1.0	1.6
		w/ DF	172g	1.43652	0.020	1.4	0.8
			23g	1.43782	0.083	0.4	0.5

* The VARIANT option used for DIF3D calculations.

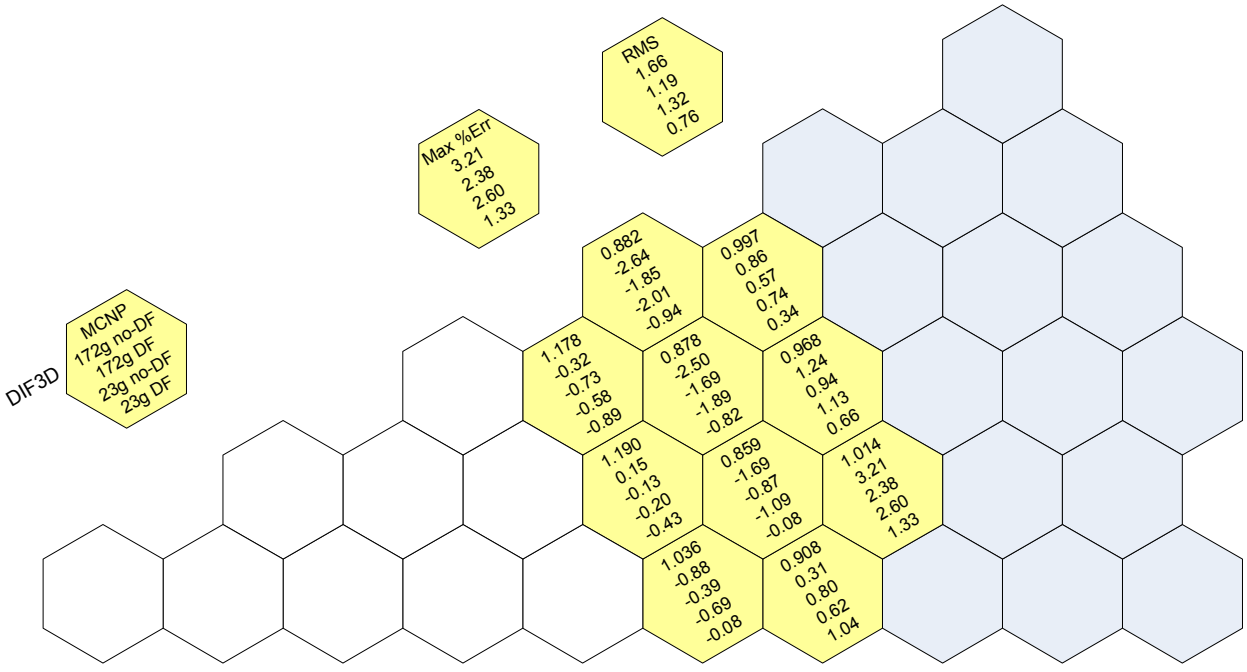

Figure 15. Power Distributions of 2-D Core Model (No-BP, No-CR, Homogenous Fuel Compact).

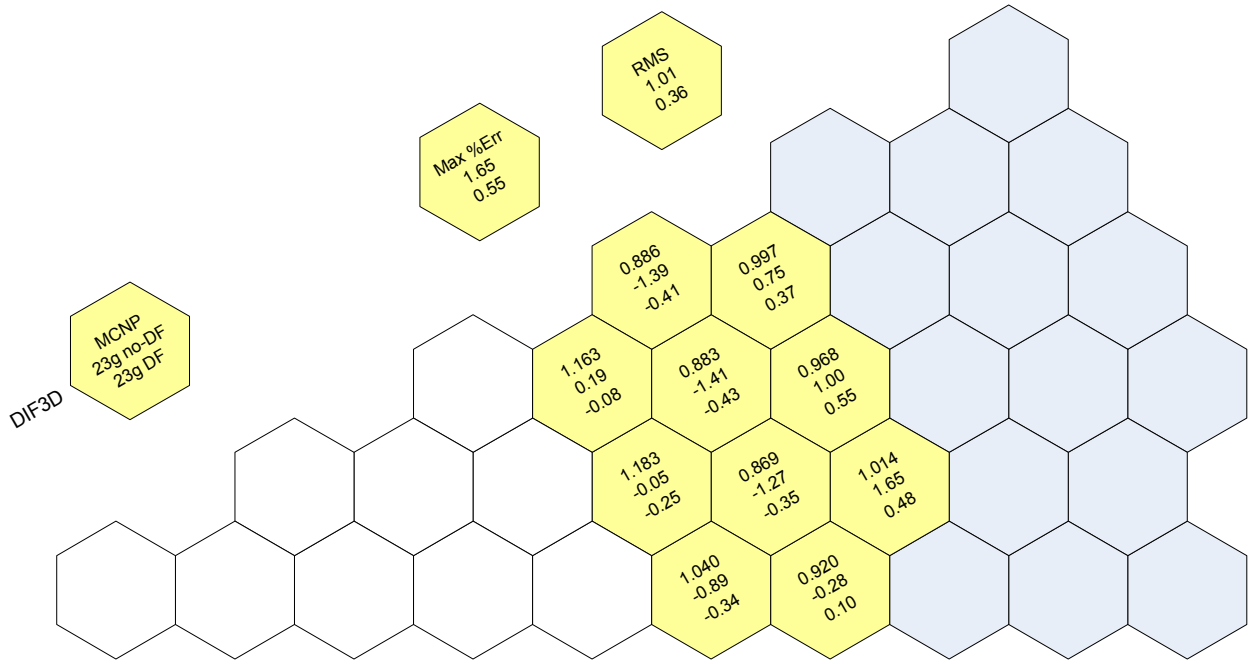

Figure 16. Power Distributions of 2-D Core Model (No-BP, No-CR, Explicit TRISO Particle Representation).

The cores with burnable poisons were also computed using MCNP and DRAGON/DIF3D. As shown in Table 9, both the multiplication factor and power distribution are improved with the application of discontinuity factors: multiplication factor differences of 0.3% and 0.6% Δρ for homogeneous fuel compact and explicit fuel particle representation, respectively, and maximum block-average power errors of 3% with both fuel compact models. The application of discontinuity factors reduces the maximum power errors by 0.5 to 0.8% and k_{eff} differences by 0.21 to 0.34% Δρ. The k_{eff} difference for the core with explicit TRISO particle representation is greater than 0.5% Δρ even when using discontinuity factors. This is partly because DRAGON calculates a k_{inf} for the single fuel element with explicit TRISO particle representation and BPs that is different by ~0.5% Δρ compared to MCNP (see Table 5). Finally, Figures 17 and 18 illustrate the differences in the core power distributions.

Table 9. Comparison of k_{eff} and Power for Core with BPs.

Fuel Compact Model	Code			k_{eff}	% Δρ	Power Error (%)	
						RMS	Max
Homogeneous Fuel Compact	MCNP			1.31077 (±0.00034)	-	-	-
	DRAGON /DIF3D*	w/o DF	172g	1.31927	0.492	1.8	-3.3
			23g	1.32161	0.626	1.5	-3.1
		w/ DF	172g	1.31520	0.257	1.5	2.8
			23g	1.31577	0.290	1.1	2.3
Explicit TRISO Particles	MCNP			1.34773 (±0.00022)	-	-	-
	DRAGON /DIF3D*	w/o DF	172g	1.36141	0.746	1.8	3.5
			23g	1.36381	0.875	1.6	3.0
		w/ DF	172g	1.35761	0.540	1.6	2.8
			23g	1.35850	0.588	1.1	2.2

* The VARIANT option used for DIF3D calculations.

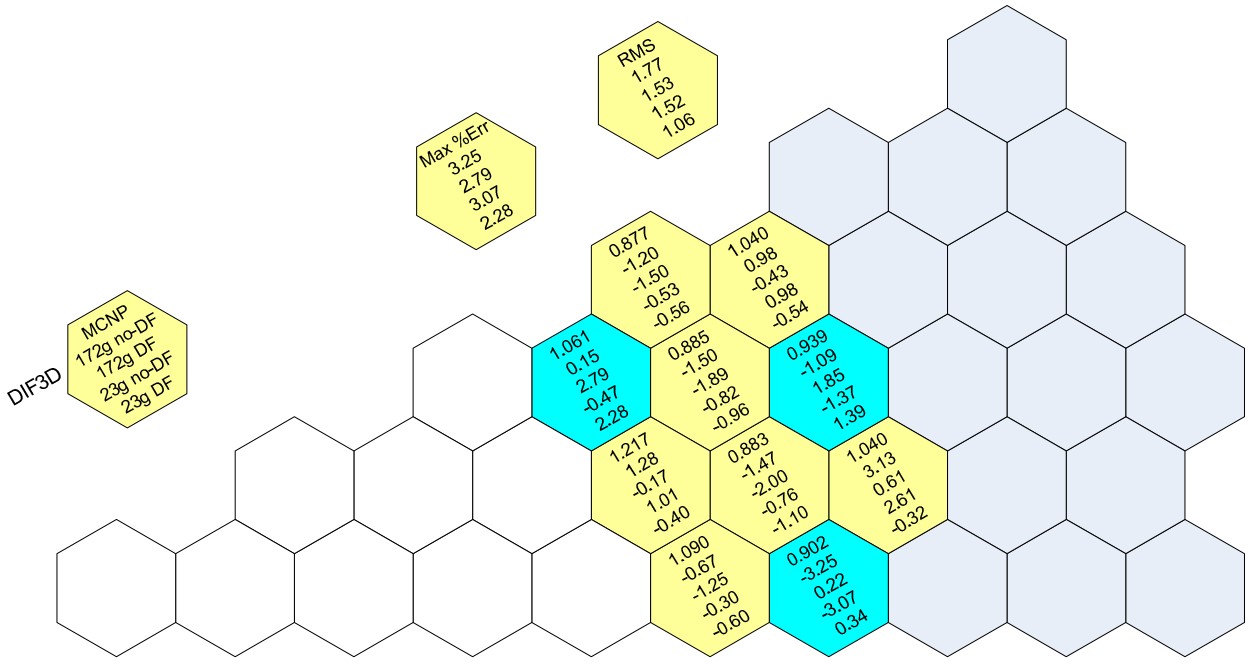

Figure 17. Power Distributions of 2-D Core Model (30 BP Blocks, No-CR, Homogeneous Fuel Compact).

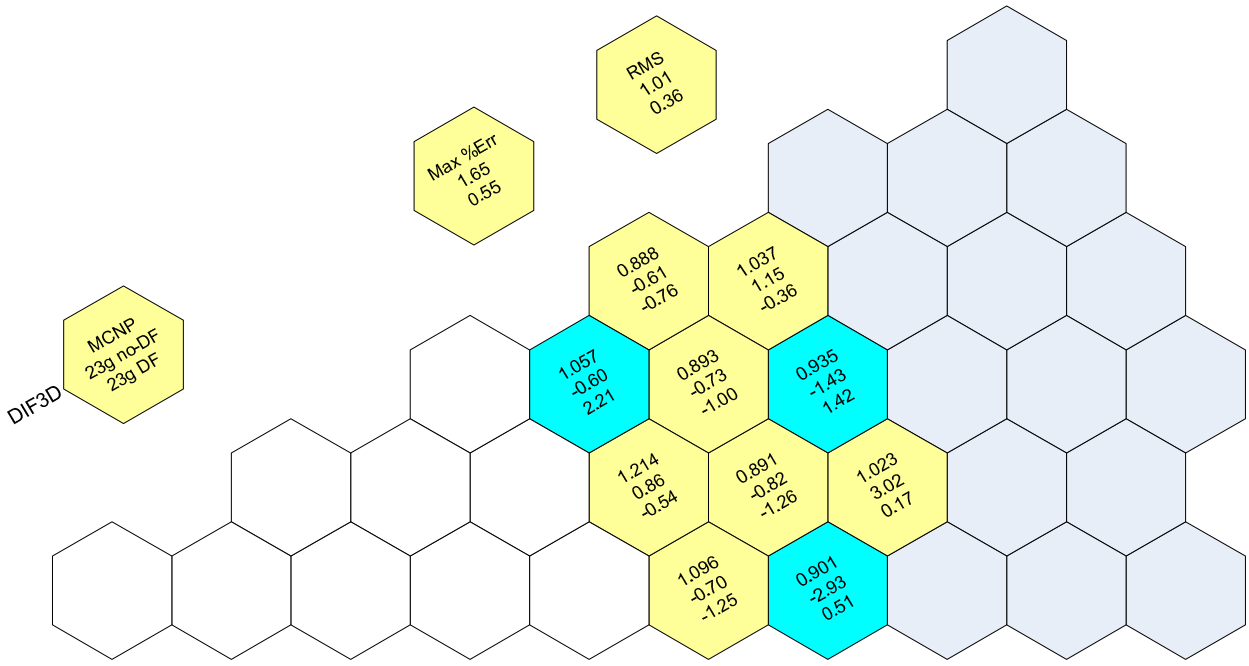

Figure 18. Power Distributions of 2-D Core Model (30 BP Blocks, No-CR, Explicit TRISO Particle Representation).

Cores with Control Rods

Using cross sections generated using the one-dimensional control rod models (Section 4.1), two types of rodded core configurations have been studied: a core with 6 control rods (CRs) fully inserted in the outer reflector region and another with 30 control rods fully inserted, as shown in Figure 19. The control rod locations were slightly modified from the original VHTR design to give cores with one-twelfth symmetry. Control rod cross sections for the core with 6 CRs are of Type A and those for the core with 30 CRs are of Types A and B (described in Section 4.1). All the cross sections for DRAGON/DIF3D calculations were adjusted with discontinuity factors using the SET approach. Thus, surface-dependent discontinuity factors have not been applied in these core calculations.

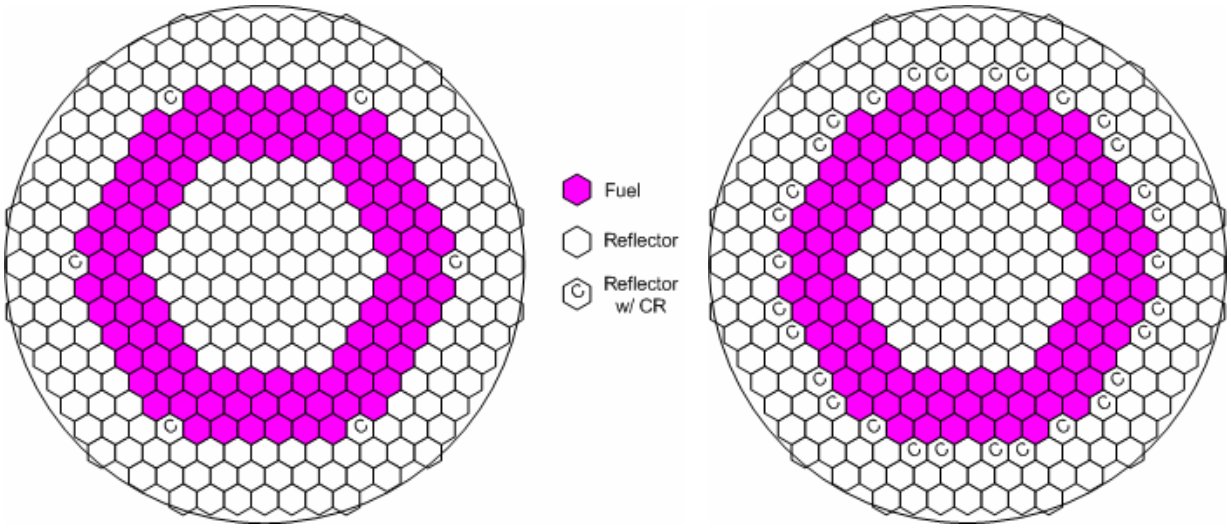

Figure 19. Two-Dimensional Core Configurations with 6 or 30 Control Rod Blocks.

Table 10 summarizes the core k_{eff} values and control rod worths obtained from MCNP and DRAGON/DIF3D calculations. The control rod worths calculated by DRAGON/DIF3D and MCNP are within 6% of each other for both cores. The 172-group DRAGON/DIF3D solutions were found to be closer to the reference MCNP solution than the 23-group solutions. For generating the 23-group cross sections in DRAGON, the infinite spectrum option was chosen since its spectrum is more representative of that in the core of interest than the critical spectrum (a different DRAGON option).

Since cross sections have been simply adjusted using a set of discontinuity factors (SET approach) instead of using surface-dependent discontinuity factors, relatively large power errors are observed for the fuel block located near rodded reflector blocks. Figures 20 and 21 show power differences up to 10% and 20% in these regions for the 6-CR and 30-CR cores, respectively. Note that the powers for the fuel blocks adjacent to the control rods are actually quite low. Additionally, the core power tilts (global differences) should be resolved by using surface-dependent nodal equivalence parameters in the future.

Table 10. Control Rod Worths of 2-D Core Models with 6 or 30 Control Rod Blocks.

Core	Code		k_{eff}	Control Rod Worth (%)	% Diff. of Rod Worth
6-CR Core	MCNP		1.36046 (±0.00034)	1.92	-
	DRAGON/ DIF3D*	172g	1.35657	1.89	-1.5
		23g	1.35799	1.81	-5.5
30-CR Core	MCNP		1.28023 (±0.00036)	6.52	-
	DRAGON/ DIF3D*	172g	1.27971	6.41	-1.8
		23g	1.28223	6.25	-4.2

* The VARIANT option used for DIF3D calculations and cross sections adjusted with discontinuity factors.

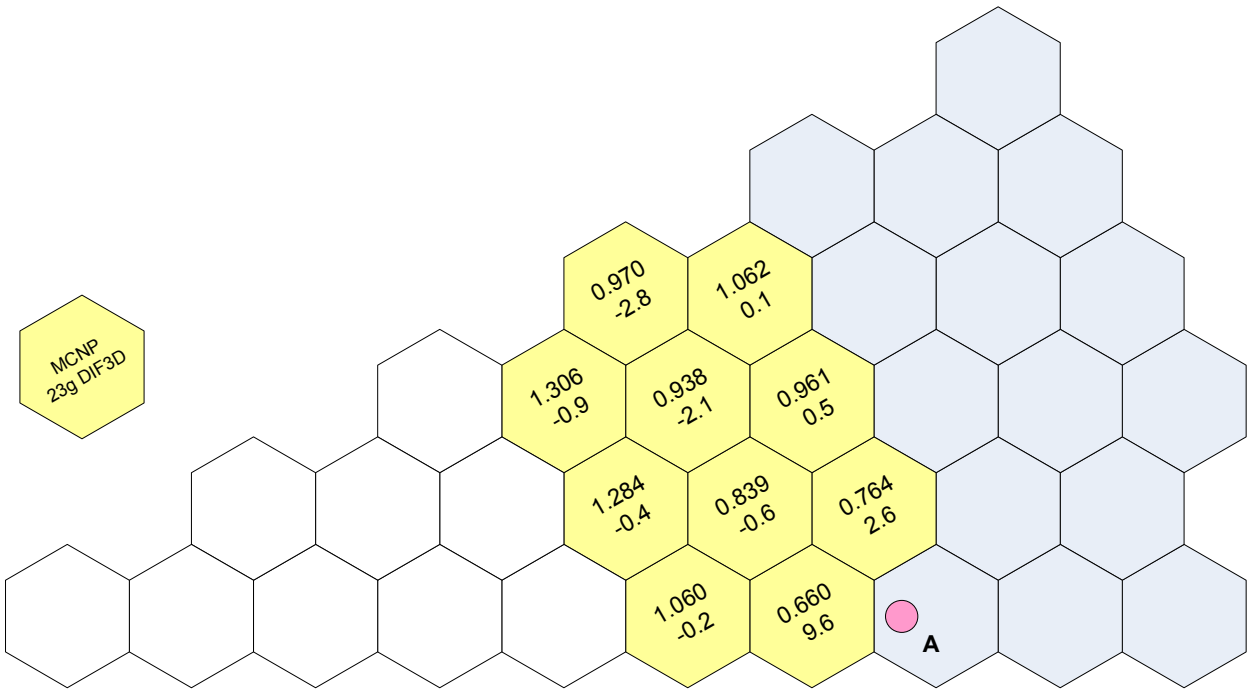

Figure 20. Power Distributions of 2-D Core Model (No-BP, 6 CR Blocks, Homogeneous Fuel Compact).

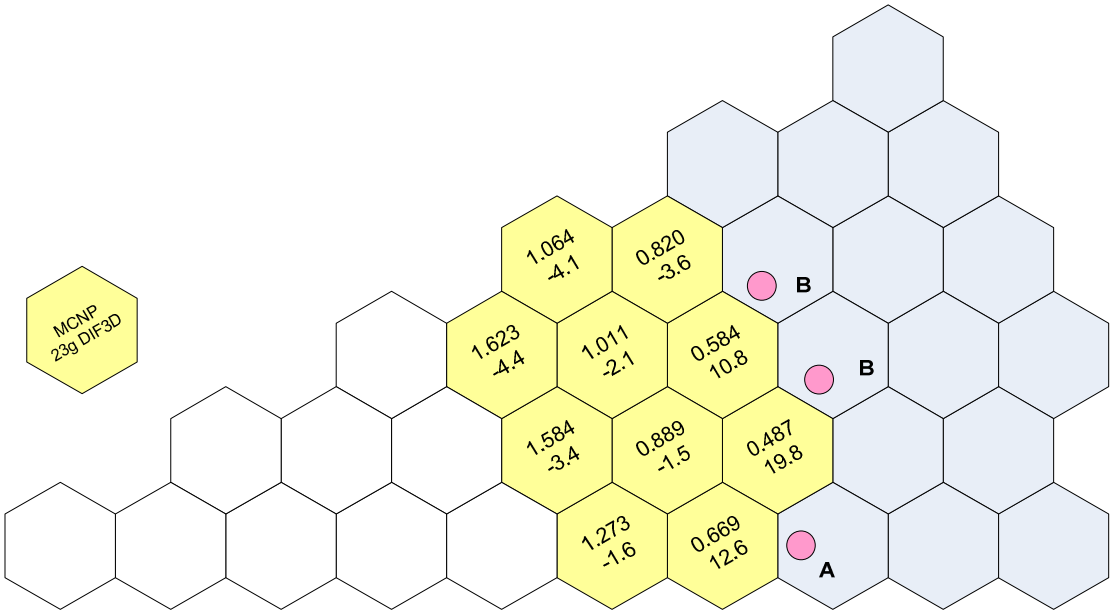

Figure 21. Power Distributions of 2-D Core Model (No-BP, 30 CR Blocks, Homogeneous Fuel Compact).

The potential to correct the core power tilts using surface-dependent discontinuity factors has been tested with the 2-D mini-core model (Type A). The nodal option of DIF3D was used for the study. As evident in Figure 22, power errors are significantly reduced by the application of surface-dependent discontinuity factors. [8] However, it was observed that the multiplication factor errors of DIF3D-nodal solutions for rodded cores were larger than those for unrodded cores because of the severe flux distortion due to the strong absorber. It was concluded that to obtain accurate multiplication factors and power distributions, the spatial approximation in DIF3D-nodal needs to be improved or a capability to handle surface-dependent discontinuity factors needs to be implemented in DIF3D-VARIANT.

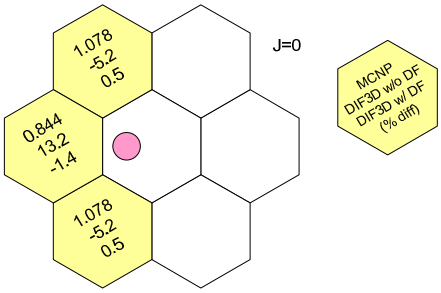

Figure 22. Comparison of Power Distributions from MCNP and DRAGON/DIF3D for 2-D Mini-Core Model with Control Rod.

4.3 Three-Dimensional Calculations

Initial Core Calculations without Thermal Feedback

The two-dimensional problems discussed in the previous section were extended to three-dimensional cores, by adding top and bottom reflectors. Although the top and bottom reflectors of the actual VHTR/NGNP design have different thicknesses (1.2 m and 1.6 m, respectively), the thickness of the bottom reflector was changed to that of the top reflector so that an axially symmetric half-core model could be used in the study.

Similarly to the two-dimensional problems, four different cores were considered, depending on the presence of BPs and the fuel compact model. The locations of BPs within a fuel block and in the core are the same as for the 2-D cores previously discussed. Fuel and radial reflector cross sections are the same as for the 2-D core calculations. Axial reflector cross sections were generated similarly to the approach used for the outer reflector cross sections. Discontinuity factors were applied to cross sections using the simplified equivalence theory approach. The VARIANT option was used for all DIF3D calculations.

Results of the DRAGON/DIF3D and MCNP calculations for the cases are summarized in Table 11. The DRAGON/DIF3D and MCNP codes predicted core multiplication factor and powers that are in good agreement. The maximum block-average power differences of the DRAGON/DIF3D solutions are within 2% of those of the MCNP solutions when discontinuity factors are applied to the cross sections. Similarly to the 2-D results, the application of discontinuity factors reduces the RMS and maximum block-average power differences as much as 0.7% and 1.4%, respectively, and the k_{eff} errors as much as 0.35% $\Delta\rho$ for most cases. Figures 23 through 26 show the power and power-error distributions for the 3-D cores.

Axial power distributions are shown in Figures 27 and 28. It is observed that in general the axial power shapes from DIF3D calculations are in good agreement with those from MCNP calculations, but axial peak powers were underestimated by ~2%, which would be acceptable. It is additionally observed that the application of discontinuity factors to the top and bottom reflectors slightly improves both the core multiplication factor and the axial power distribution. This is because the core is quite high such that the small perturbations at the axial core boundaries (introduction of DFs) do not much affect the overall core characteristics.

Table 11. Comparison of k_{eff} and Power for 3-D Core Models.

Fuel Compact Model	Code			k_{eff}	% Δ ρ	Power Error (%)	
						RMS	Max
Homogeneous Fuel Compact	No-BP	MCNP		1.38622 (±0.00012)	-	-	-
		DRAGON/ DIF3D*	w/o DF	1.38705	0.043	1.2	2.3
			w/ DF	1.38074	-0.286	0.5	-1.2
	BP	MCNP		1.30038 (±0.00012)	-	-	-
		DRAGON/ DIF3D*	w/o DF	1.31105	0.626	1.5	2.7
			w/ DF	1.30512	0.279	0.9	1.8
Explicit TRISO Particles	No-BP	MCNP		1.42500 (±0.00021)	-	-	-
		DRAGON/ DIF3D*	w/o DF	1.43160	0.323	1.1	1.9
			w/ DF	1.42575	0.037	0.6	1.0
	BP	MCNP		1.33776 (±0.00022)	-	-	-
		DRAGON/ DIF3D*	w/o DF	1.35273	0.827	1.7	3.1
			w/ DF	1.34734	0.532	1.1	1.7

* The VARIANT option with 23 group cross sections used for DIF3D calculations.

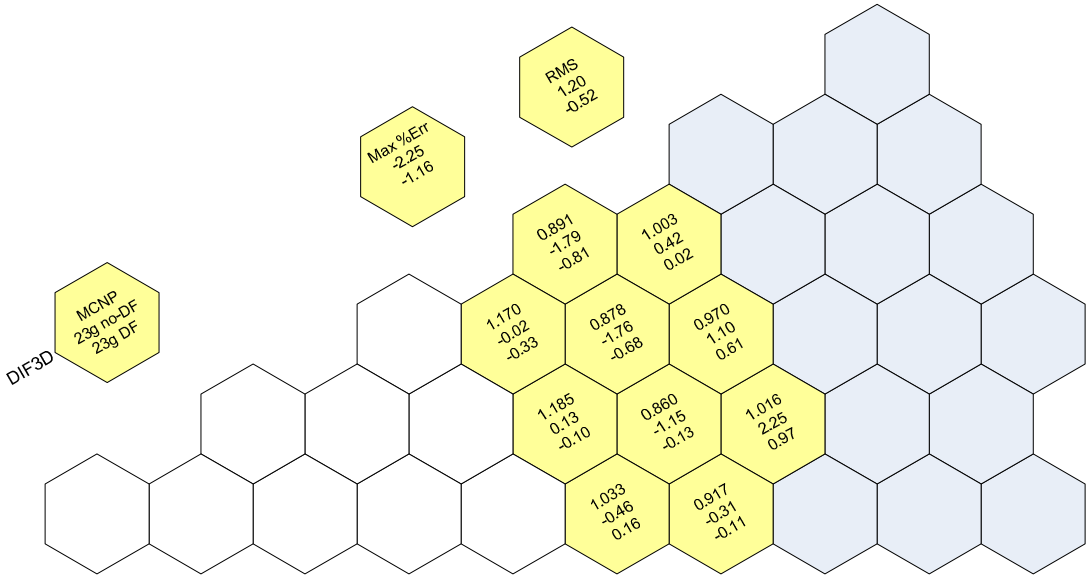

Figure 23. Radial Power Distributions of 3-D Core Model (No-BP, No-CR, Homogeneous Fuel Compact).

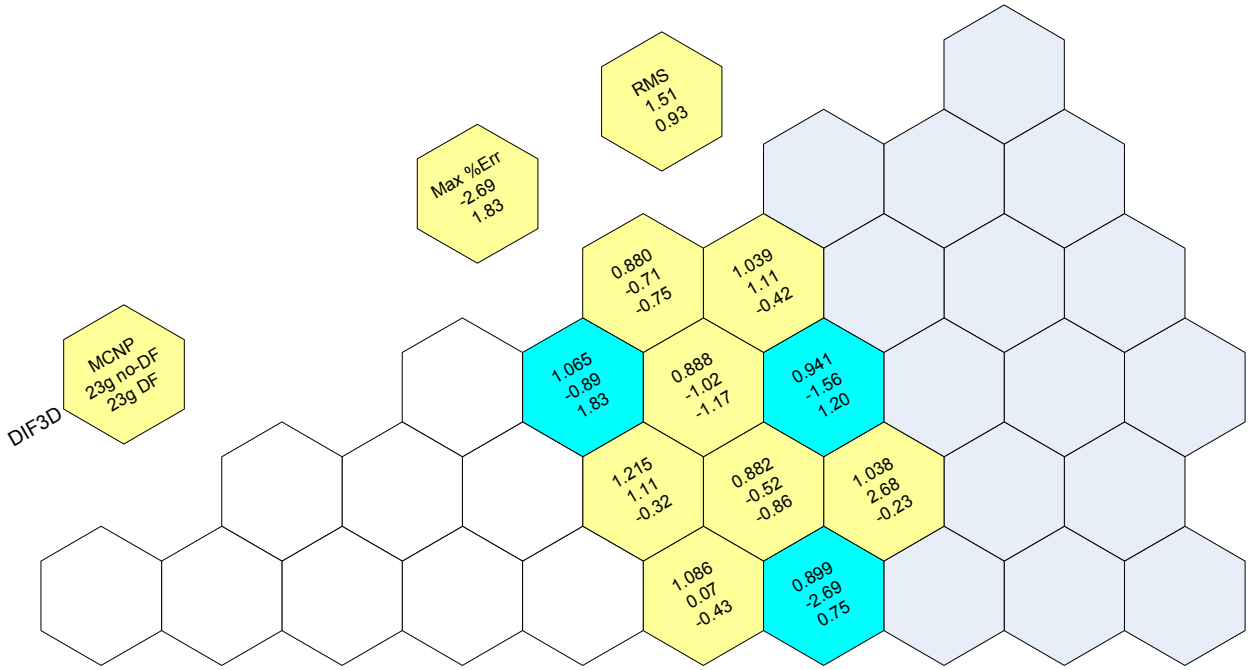

Figure 24. Radial Power Distributions of 3-D Core Model (30 BP Blocks, No-CR, Homogeneous Fuel Compact).

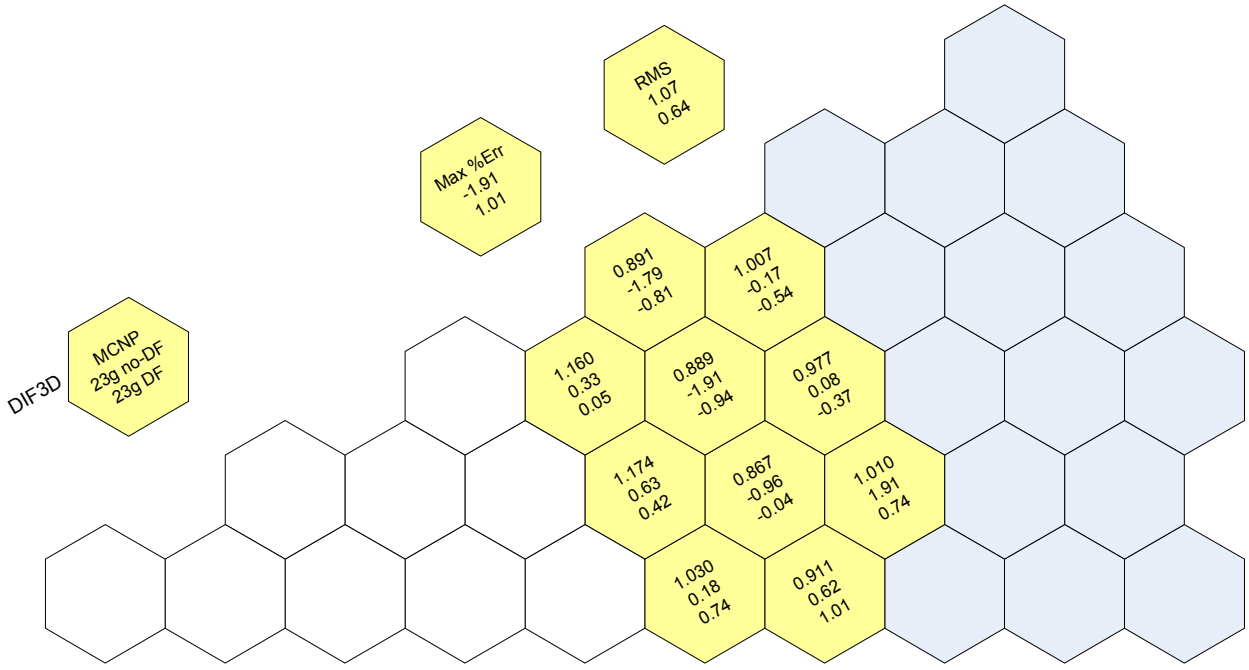

Figure 25. Radial Power Distributions of 3-D Core Model (No-BP, No-CR, Explicit TRISO Particle Representation).

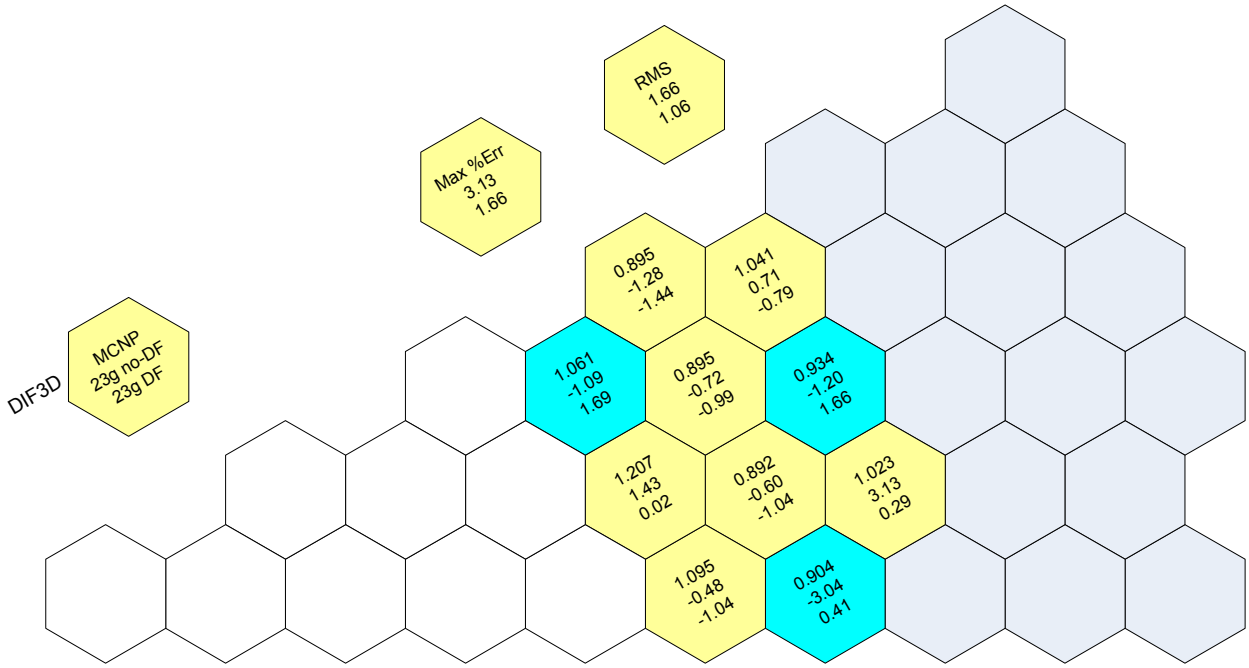

Figure 26. Radial Power Distributions of 3-D Core Model (30 BP Blocks, No-CR, Explicit TRISO Particle Representation).

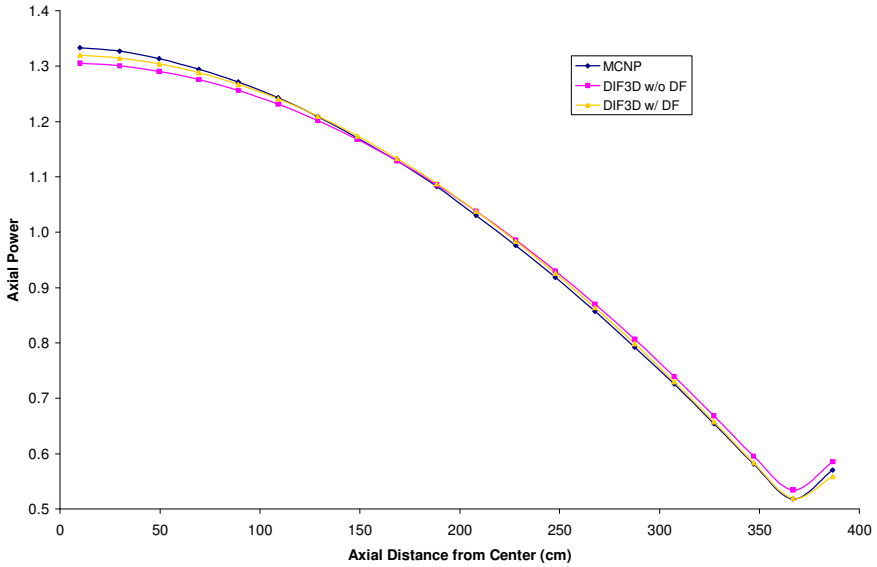

Figure 27. Axial Power Distributions of 3-D Core Model (No-BP, No-CR, Homogeneous Fuel Compact).

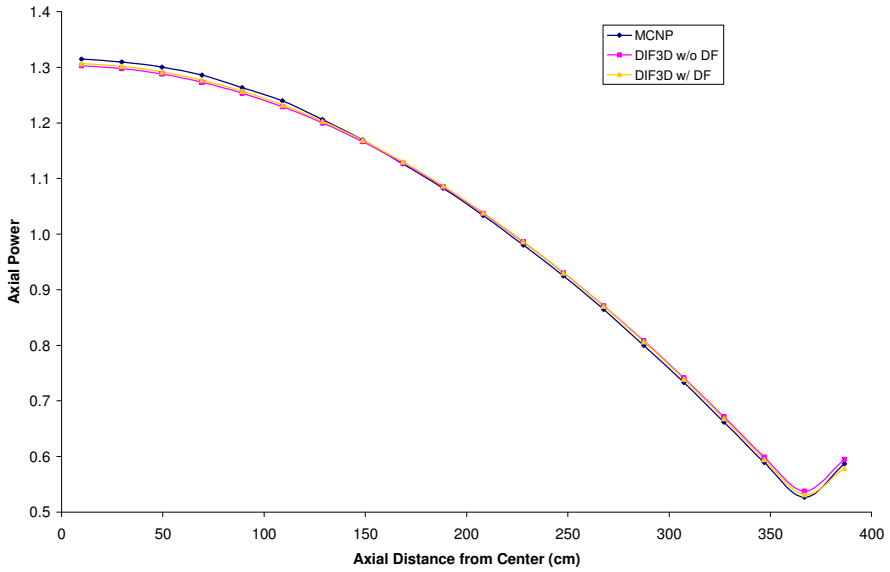

Figure 28. Axial Power Distributions of 3-D Core Model (30 BP Blocks, No-CR, Homogeneous Fuel Compact).

Thermal Feedback Calculation

The code suite has been used to evaluate the impact of thermal feedback on 3-D core results. Core solutions with and without the use of the thermal feedback option were compared for this purpose. The core was axially divided into 20 thermal regions to accurately represent the impact of cross sections changes with the axial temperature profile.

Figure 29 displays the different profiles obtained for the axial power and temperature distributions at the beginning of cycle (BOC) with and without feedback. No reference solution has been generated for this case; the MCNP capabilities that are available do not have any thermal feedback models. Note that conductivities of fuel compact and graphite were assumed to be constant with temperature for this comparison. The results show the importance of representing the thermal feedback ("T/H" case in Figure 29). The core axial power peak is slightly higher with feedback. More importantly, the location of this peak is also quite different; this core location is important as it provides an indication of where the core axial power peak could be suppressed by design (e.g., using BPs), if it is limiting. The non-uniform axial

temperature profiles also show the impact of the feedback option. Without thermal feedback these profiles are uniform.

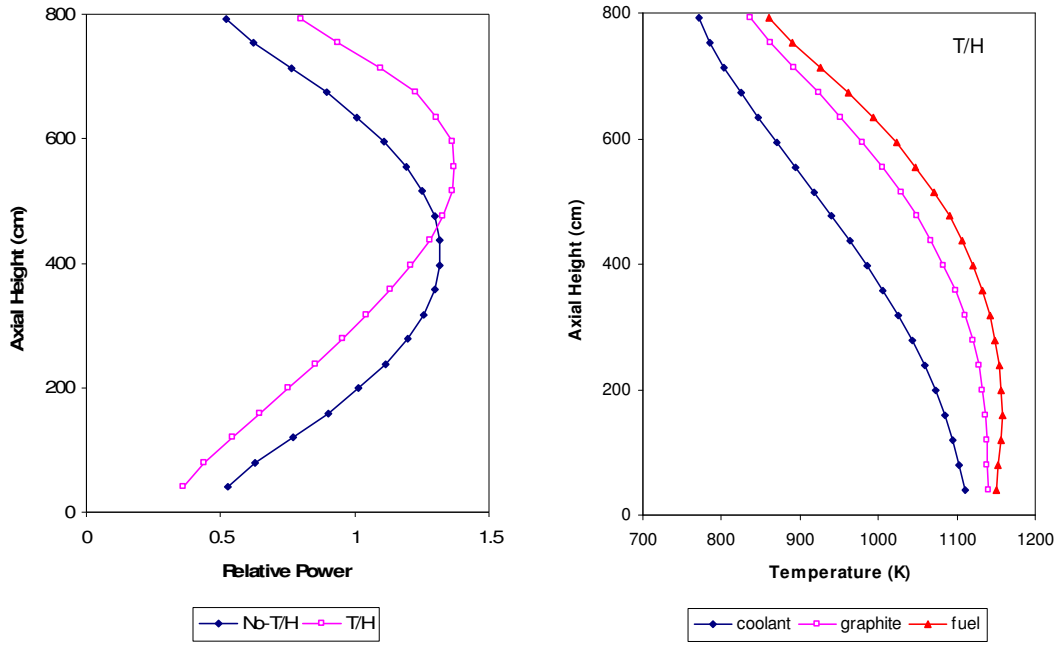

Figure 29. Axial Power and Temperature Profiles from REBUS-3/DIF3D.

5.0 CONCLUSIONS

Previous evaluations have indicated that the REBUS-3, DIF3D, and DRAGON codes could be used as foundation for a deterministic code suite for the accurate and efficient analysis of prismatic Very High Temperature Reactor (VHTR) cores. Starting in FY 2006, enhancements are being made to the REBUS-3/DIF3D/DRAGON code suite to provide the necessary capabilities and functionalities. This report has focused on the REBUS-3/DIF3D whole-core analysis capabilities for the code suite. A companion report (ANL-GenIV-075), issued in August 2006, [8] focused on the DRAGON code capabilities and cross section generation.

Currently, cross sections generated using the DRAGON lattice code are employed in the whole-core calculations. The cross sections variations as a function of burnup and temperatures are provided to the code suite in tabular form. The tabulated cross sections are stored in one ISOTAB file which has a hierarchical structure with isotope, burnup, and temperature. A large number of fission products could be merged into a single lumped fission product to save space, memory, and computing time in REBUS-3 fuel cycle analysis without sacrificing the accuracy of the depletion solution. However, a few fission products such as I, Xe, Pm, and Sm, are always explicitly defined since their number densities need to be accurately estimated with burnup due to their significant reactivity impacts.

For handling the ISOTAB file in REBUS-3/DIF3D, new modules, namely, NEUTRONXS, COMPACTSCAT, and GENERALISOTOPE, have been developed using FORTRAN 90/95 object-oriented data structures. The NEUTRONXS module provides a new cross section storage procedure, while the GENERALISOTOPE module constructs a complete set of microscopic cross section data for all isotopes. The COMPACTSCAT module contains a single block of banded scattering data which makes it possible to reduce the memory usage and easily transfer data from and to disk. Additionally, the DIFFERENTIALBURNUP routine has been developed to obtain material- and stage-dependent burnups for use in the calculation of burnup-dependent cross sections.

For thermal feedback calculations, a simple heat conduction model has been developed and implemented in REBUS-3. The axial conduction term was neglected in the model's

formulation because the axial temperature gradient is significantly smaller that the radial temperature gradient. It was found that average fuel and graphite temperatures can be accurately estimated compared to STAR-CD results by simply weighting two temperature values (centerline and surface temperatures for fuel and two surface temperatures for graphite). Additionally, it was observed that for the steady-state thermal-fluid calculation, the pressure variation along the coolant channel can be neglected. The ONEDTHERMOHYDRAULICS routine has been developed using FORTRAN 90/95 programming to perform the thermal feedback calculations in REBUS-3. A new set of input cards in the A.THERM ASCII file have been defined for providing the necessary thermal property inputs.

Control rod cross sections are treated as an isotope using a delta-macroscopic format. New input data for control rod configuration have also been defined and added to the A.THERM file. Additionally, the ATHERM and FILL_IN_COMPXS routines of REBUS-3 have been updated to support the simulation of control rods in prismatic VHTRs.

The need for surface-dependent discontinuity factors in nodal calculations necessitated the modification of several routines in the DIF3D-nodal Hex-Z version of the code (DIF3D-nodal). The original implementation of surface-dependent discontinuity factors for surface-average fluxes, currents, and moments was simplified so that discontinuity factors for surface currents only could be used, as typically utilized for thermal reactor analysis. It was originally thought that using surface-dependent discontinuity factors in the DIF3D-nodal option would give good accuracy for all core configurations. This has not been the case for rodded configurations, due to the relatively poor transverse leakage approximation made for the nodal option (particularly when a large hexagonal pitch is used in the code).

With fuel, reflector, and control rod cross sections generated by the approaches discussed in Reference 8, as well as the routines developed and modified in this work, two- and three-dimensional core calculations with and without burnable poisons or control rods were performed using the code suite. Results were compared with corresponding MCNP solutions. Generally, REBUS-3/DIF3D results for the core multiplication factor and power distribution were found to be in good agreement with MCNP results particularly when discontinuity factors are applied. It was also shown that the DIF3D-VARIANT option provides a better spatial solution in its

diffusion approximation. The application of discontinuity factors reduced fuel block average power differences by as much as 0.5 to 1.4% and core multiplication factor differences by as much as 0.20 to 0.35% $\Delta\rho$ for cores with or without burnable poisons. In addition, it was observed that control rod worths could be estimated within an acceptable range compared to MCNP results. However, the core power tilt (particularly in the rodded zones) needs to be improved by introducing surface-dependent discontinuity factors. The improved performance with surface-dependent discontinuity factors was shown at the mini-core level. It was therefore recommended that a routine for surface-dependent discontinuity factors be provided for the VARIANT option of DIF3D (DIF3D-VARIANT) or the spatial approximation of the nodal option (DIF3D-nodal) be improved in the future.

The 3-D core calculations with and without thermal feedback indicated the significant impact of having a thermal feedback model. The accuracy of the current thermal feedback model in the code suite needs to be verified in the future using reference calculations coupling neutronic and thermal-fluid models. Additionally, the thermal feedback routine should be extended to equilibrium-cycle depletion calculations; it currently works for the traditional non-equilibrium cycle depletion calculations.

REFERENCES

1. R. C. Potter et al., "Gas Turbine-Modular Helium Reactor (GTMHR) Conceptual Design Description Report," GA Report 910720, Revision 1, General Atomics, July 1996.

2. P. E. MacDonald et al., "NGNP Preliminary Point Design – Results of Initial Neutronics and Thermal-Hydraulic Assessment," **INEEL/EXT-03-00870** Rev. 1, Idaho National Engineering and Environmental Laboratory, September 2003.

3. T. A. Taiwo, W. S. Yang, M. A. Smith, T. K. Kim, and H. S. Khalil, "Assessment of Reactor Physics Codes for Analysis and Design of the Very High Temperature Reactor (VHTR)," Argonne National Laboratory Gen IV Report, September 30, 2004.

4. T. K. Kim, W. S. Yang, T. A. Taiwo, and H. S. Khalil, "Whole-Core Depletion Studies in Support of Fuel Specification for the Next Generation Nuclear Plant (NGNP) Core," Argonne National Laboratory Gen IV Report, July 30, 2004.

5. G. Marleau, et al, "A User Guide for DRAGON," Technical report **IGE-174** Rev. 4, Ecole Polytechnique de Montréal, September (1998).

6. B. J. Toppel, "A User's Guide to the REBUS-3 Fuel Cycle Analysis Capability," **ANL-83-2**, Argonne National Laboratory (1983).

7. R. D. Lawrence, "The DIF3D Nodal Neutronics Option for Two- and Three-Dimensional Diffusion Theory Calculations in Hexagonal Geometry," **ANL-83-1**, Argonne National Laboratory (1983).

8. C. H. Lee, Z. Zhong,, T. Taiwo, W. Yang, M. Smith, and G. Palmiotti, "Status of Reactor Physics Activities on Cross Section Generation and Functionalization for the Prismatic Very High Temperature Reactor, and Development of Spatially-Heterogeneous Codes," **ANL-GenIV-075**, Argonne National Laboratory (2006).

9. J. F. Briesmeister, Editor, "MCNP^{TM} - A General Monte Carlo N-Particle Code, Version 4C," Los Alamos National Laboratory, **LA-13709-M**, March 2000.

10. G. Palmiotti, E. E. Lewis, and C. B. Carrico, "VARIANT: VARIational Anisotropic Nodal Transport for Multidimensional Cartesian and Hexagonal Geometry Calculation," **ANL-95/40**, Argonne National Laboratory (1995).

11. STAR-CD, CD-ADAPCO Inc., Melville, New York.

12. P. J. Finck and K. L. Derstine, "The Application of Nodal Equivalence Theory to Hexagonal Geometry Lattices", Proceedings of the International Topical Meeting Advances in Mathematics, Computations and Reactor Physics, Pittsburgh, PA., Vol. 4, pp. 16.1 4-1 (1991).

13. K. S. Smith, “Spatial Homogenization Methods for Light Water Reactor Analysis,” Ph.D. Thesis, Massachusetts Institute of Technology (1980).

14. K. Koebke, “A New Approach to Homogenization and Group Condensing,” Proc. IAEA Specialists’ Mtg. Homogenization Methods in Reactor Physics, Lugano, Switzerland, **IAEA-TECDOC-231**, 303 (1978).